Chapter 6

Summary

To examine the role of various intervening processes in controlling the upper ocean thermal structure in the central Arabian Sea, a 1-D mixed-layer model based on turbulent closure scheme is forced by atmospheric fluxes and advective heat fluxes over the one-year period of the JGOFS time-series starting from mid-October 1994 in the central Arabian Sea at (61.5^{o}E & 15.5^{o}N). Atmospheric forcing data are available from the moored array observations (Weller et al. [2]). The horizontal advective contributions at the study location are available from two different sources. The first estimate is based on local *in situ* measurements (as earlier estimated by Fischer et al. [4]). The second estimate is based on optimally interpolated satellite SST field and *in situ* currents. The vertical velocity, as in all oceanography problem, poses a challenge. Two possible approaches have been considered for the diagnostic analysis. In the first approach, the model was used to predict the temperature profile (using atmospheric fluxes and estimates of horizontal and vertical advection). In the second approach, the observed temperature profiles (and atmospheric fluxes and estimates of horizontal advection) were used to force the model in order to predict the vertical velocity.

Besides the main experiments carried out using the above two approaches, additional experiments were also performed mainly for two purposes: (i) to support the analysis of the results obtained from the main experiments, and (ii) to examine the role of auxiliary parameters (salinity and biomass) in the seasonal evolution of upper-ocean temperature. Finally, model-based heat-budget analysis for the four monsoon seasons: winter, spring, summer, and autumn has been carried out. The following are the three important conclusions of the thesis.

(1) Vertical advection is an important process, as important as atmospheric fluxes and horizontal advection, throughout the year in controlling the upper ocean thermal structure and the heat budget of the central Arabian Sea.

(2) The general trends of ML deepening and SST cooling in the central Arabian Sea during the NE monsoon are due to buoyancy driven convective entrainment mixing, whereas the trends of ML deepening and SST cooling during the SW monsoon are due to both wind driven mixing and buoyancy driven convective mixing. However, the observed trends of ML and SST during the whole year can only be reproduced when all the intervening process are accounted for: advection together with atmospheric fluxes.

(3) Ocean dynamics plays a primary role in controlling the thermodynamics of the upper ocean in the central Arabian Sea, whereas salinity and phytoplankton biomass concentration evolution do not have a significant local control over the thermal structure.

(4) Some results of the present study have their validity limited by the uncertainties in Fischer-based horizontal advective heat fluxes. The deployment of a four/five mooring system to quantify the contributions of horizontal variability is believed not to be satisfactory as far as quantitative estimation is concerned. The information obtained from the central mooring in combination with satellite altimeter imagery proves to be at least as good, and may be better.

At the end of this thesis, we do not know whether the conclusions obtained for the central Arabian Sea are still valid in other parts of the Arabian Sea. This issue still remains an open question. This can be answered by achieving similar model-based diagnostic studies or by carrying out a basin scale study using a 3D model.

This model can be used for studies similar to those presented in this thesis to understand the eastern and southeastern Arabian Sea, where time-series observation were carried out during the Arabian Sea Monsoon Experiment (ARMEX) during 2002–2003.

Thermodynamics of the ocean influences the biogeochemical system of the ocean environment. Another perspective is to couple a biogeochemical model to an upper ocean thermodynamical model to perform a simulation of carbon and nitrogen fluxes along an annual cycle in the central Arabian Sea.

Appendix A

Equation of state for sea water

UNESCO formula (Millero and Poisson [121]) for density of sea water:

$$\rho = \rho_0 + A \cdot S + B \cdot S^{3/2} + C \cdot S^2 \tag{A.1}$$

$$A = 8.24493 \times 10^{-1} - 4.0899 \times 10^{-3} T + 7.6438 \times 10^{-5} T^2 - 8.2467 \times 10^{-7} T^3 + 5.3875 \times 10^{-9} T^4 \tag{A.2}$$

$$B = -5.72466 \times 10^{-3} + 1.0227 \times 10^{-4} T - 1.6546 \times 10^{-6} T^2 \tag{A.3}$$

$$C = 4.8314 \times 10^{-4} \tag{A.4}$$

$$\rho_0 = 999.842594 + 6.793952 \times 10^{-2} T - 9.095290 \times 10^{-3} T^2 + 1.001685 \times 10^{-4} T^3 - 1.120083 \times 10^{-6} T^4 + 6.536332 \times 10^{-9} T^5 \tag{A.5}$$

Where T is in Deg C, S is in psu, and ρ_0 and $\rho$are in Kg/m^3.

Appendix B

Results of the auxiliary experiments

The experiments carried out in Chapter 4 to predict the upper ocean thermal structure in the central Arabian Sea, did not consider salinity variations. The inaccuracy in the predicted salinity may affect the results. The effect of salinity will be examined below in section B.1 by forcing the model with *in situ* salinity measurements.

Similarly, the attenuation of solar light in the main experiments corresponds to a constant clear oceanic water type-I (Jerlov [102]). The effect of a varying chlorophyll profile will be examined in section B.2, by forcing the model with *in situ* measurements using a spectral light attenuation scheme.

In all the experiments achieved (Chapter 4), the atmospheric forcing fluxes from the JGOFS mooring were used. How does the mixed layer respond to the individual forcing fluxes? These response will be examined in section B.3.

B.1 Impact of salinity

Salinity plays potential role in controlling the temperature structure by affecting the density field. The numerical experiments carried out in Chapter 4 did not account for the impact of salinity. The governing equation of the salt balance did not include the impact of advective processes (due to lack of data). As a consequence the predicted salinity structure differs significantly from the observed value (see Fig. B.1). At the surface, the differences between the observed and predicted salinity are large during the SW monsoon (upto 0.8 psu). In sub-surface the differences are large during January to mid-July (upto -0.8 psu).

To examine the role of salinity on the temperature structure, two simulations similar to S3c are carried out. The first simulation (S3Sa) is carried out by prescribing to the model a constant

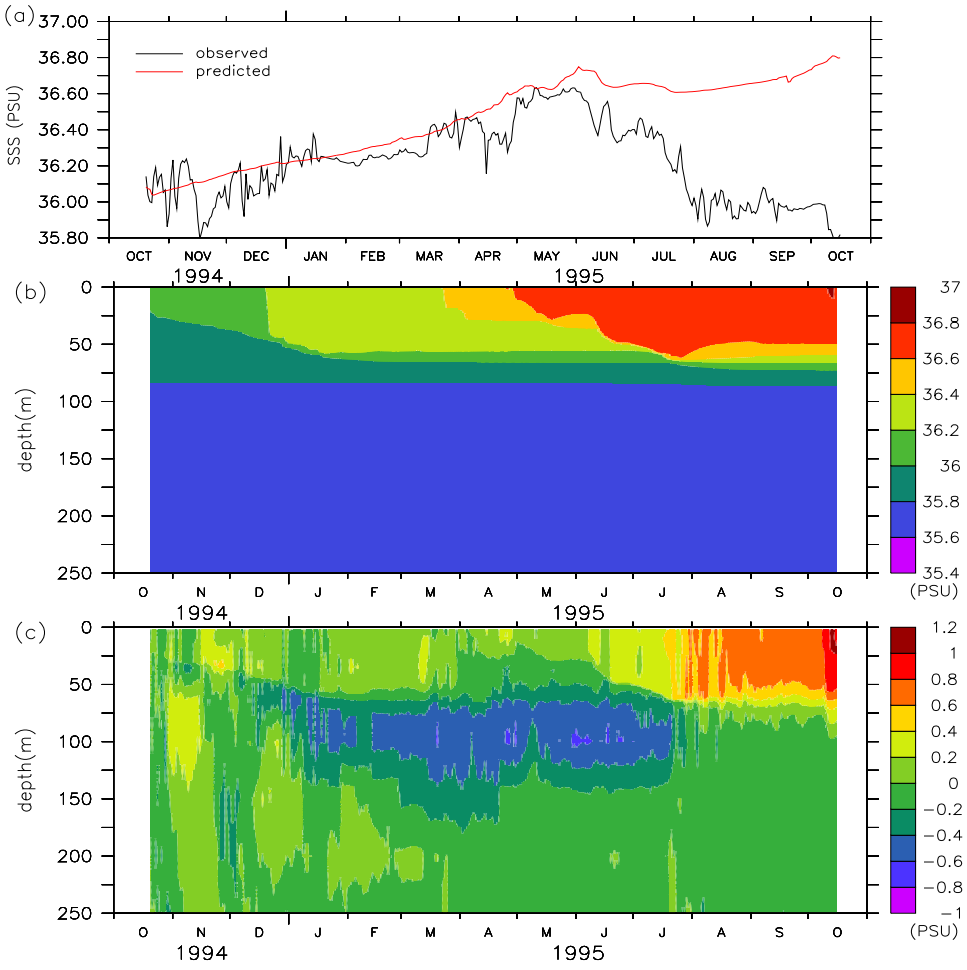

Figure B.1: Results of the simulation S1: (a) Sea Surface Salinity (SSS) (red) is compared with the observed SSS (black), (b) vertical structure of predicted salinity, (c) modeled minus observed salinity.

salinity (36 psu) and the second simulation (S3Sb) is carried out by prescribing to the model the observed salinity field. The results of both simulations are presented in the Fig. B.2. The figures show that the simulations are mostly identical, which implies that the salinity variation has a secondary role in controlling the upper ocean thermal structure in the central Arabian Sea.

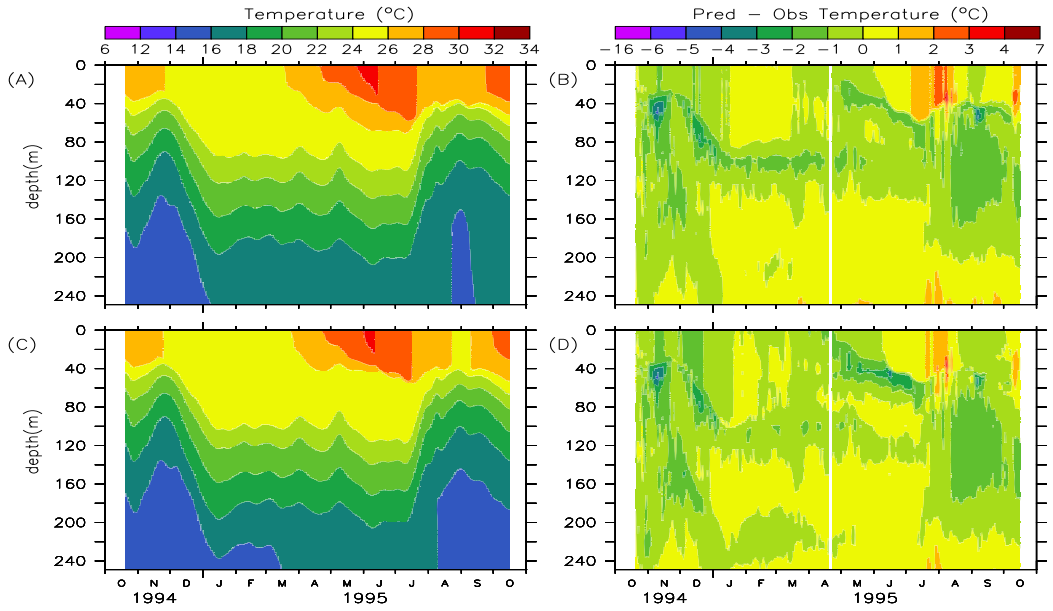

Figure B.2: Result of sensitivity experiments examining the effect of salinity on the upper ocean thermal structure in the central Arabian sea: (A) simulated temperature field when the TKE model is forced with constant salinity (36 psu); (B) same as (A), but for difference between predicted and observed temperature filed; (C) simulated temperature field when the TKE model is forced with observed salinity filed; (D) same as (C), but for difference between predicted and observed temperature field.

B.2 Impact of biomass

Biomass (chlorophyll concentration) influences the thermal structure. The process responsible is the vertical attenuation of solar irradiance. To examine the impact of chlorophyll, a spectrally resolved bio-optical model of solar irradiance $I(z)$ (Appendix-C.3) was selected and embedded in the mixed-layer model in place of the default double exponential function of $I(z)$ (see Eqn. 3.21). Simulations similar to simulation S1 (section 4.1.1) are carried out as follows. In the first simulation (S1a) the bio-optical model is forced with observed chlorophyll profiles (presented in the Fig. 3.7). In the second simulation (S1b) the model is forced with a low and constant uniform chlorophyll concentration of 0.1 mg m^{-3}. In the third simulation (S1c), the model is forced with a relatively high constant uniform chlorophyll concentration of 0.5 mg m^{-3}. The fourth simulation (S1w) is carried out for the case of pure oceanic water with zero chlorophyll concentration. The results of these simulations are compared with the results from the simulation S1 (achieved in the chapter 4.1.1 for the case of Jerlov's water type-I) in the Fig. B.3.

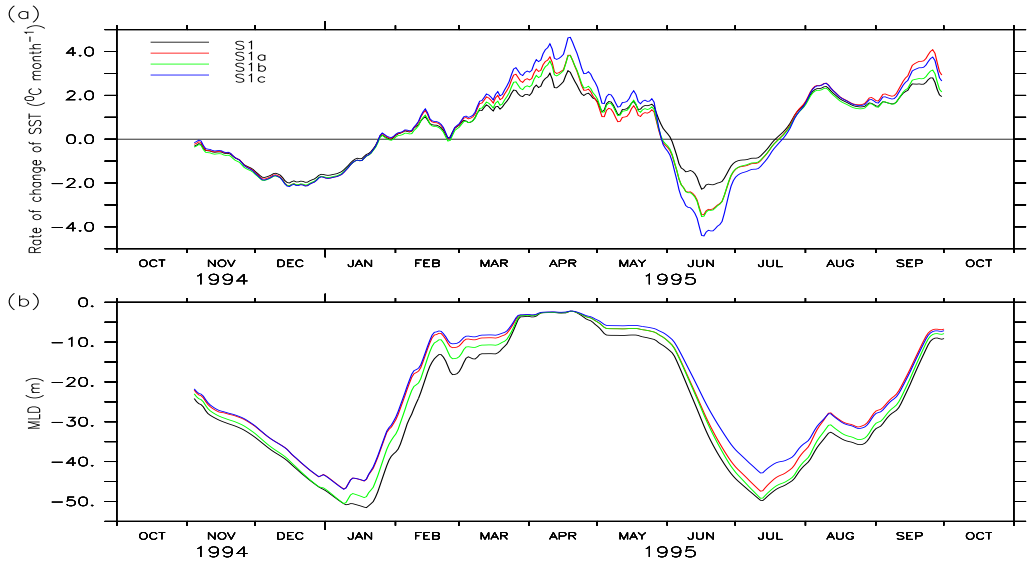

Figure B.3: Comparing between the results from simulations S1, S1a, S2b, and S2c to see the impact of biomass variation on the upper ocean thermal structure in the central Arabian sea. (a) The rate of change of predicted SST and (b) the predicted MLD. Data are smoothed in the figure with one month low pass filter.

The rate of change of predicted SST (Fig. B.3a) and predicted MLD (Fig. B.3b) of the simulations S1a, S1b, and S1c parallel the simulation S1. The difference between the rate of change of predicted SST among various simulations are upto 1°C month^{-1} during April, upto 2 °C month^{-1}during June, and upto 1 °C month^{-1} during September to early October and the difference is small (0.5°C month^{-1}) during remaining period of the year. The difference between the predicted MLD among the various simulations are upto 8 m during the year except April when the differences are negligible.

Among all the simulations: S1a, S1b, and S1c, S1b (based on 0.1 mg m^{-3}) is the nearest to the simulation S1 (based on Jerlov water type-I). Differences between the rate of change of SST of the two simulations (S1 and S1b) are upto 1°C month^{-1} only during June and relatively small during remaining period of the year. Differences between the MLD of the two simulations are upto 4 m only. Similarly, the simulation S1a (corresponding to observed chlorophyll concentration) is nearest to the simulation S1c (corresponding to large chlorophyll concentration: 0.5 mg m^{-3}) during most of the period of the year except during June when S1a almost coincides with S1b (corresponding to low chlorophyll concentration: 0.1 mg m^{-3}). It is worth noting that observed chlorophyll concentration is less than 0.3 mg m^{-3} during the early half of June.

The difference of the simulations S1b (case of low chlorophyll concentration: 0.1 mg m^{-3})

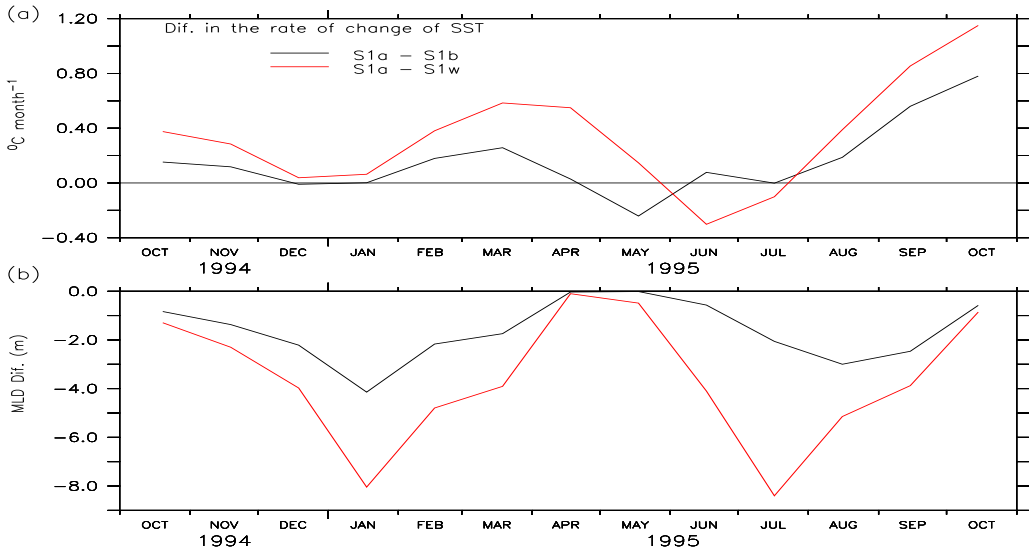

Figure B.4: The difference of the simulations S1b and S1w from the simulation S2b: (a) difference between the rate of change of the predicted SSTs and (b) difference between the predicted MLDs.

and S1w (for pure oceanic water i.e., zero chlorophyll concentration) from the simulation S1a (the case of observed chlorophyll concentration) are presented in Fig. B.4.

The difference of the simulation S1b from the simulations S1a (see Fig. B.4) indicates that the mixed layer depth (MLD) lowers by 4 m during the NE monsoon, and 3 m during the SW monsoon when the role of chlorophyll is accounted for, compared to the situation of a constant low chlorophyll (0.1 mg m^{-3}) water. During both these periods the impact on the sea surface temperature (SST) is less than 0.2 ^{0}C month^{-1}. During the spring inter-monsoon the mixed layer is shallow (MLD $\leq$ 20 m), and the impact of chlorophyll on SST is also less than 0.2 ^{0}C month^{-1}. In contrast, during the Autumn inter-monsoon the mixed layer is also shallow, but the impact of chlorophyll concentration in SST is relatively large: 0.5 ^{0}C month^{-1}. Although it seems that local impact of chlorophyll variation in the mixed layer thermodynamics is relatively large during the Autumn inter-monsoon compared to the rest of the period of the year, the impact is not significant unlike the earlier studies by Sathyendranath et al. [36] who reported biological (chlorophyll variation) heating is almost 4 ^{0}C month^{-1}during the month of August in the Arabian Sea, however, their study location was different than our study location. This result can be compared to the study carried out by Babu et al. [112] at the same study location. Unlike their study, our study shows only 2 m deepening of the ML during the month of August (which is only 3 % of the observed MLD) and its impact in SST change is less only .4 ^{0}C month^{-1} in contrast to their conclusion that biological heating impact is significantly strong during this period. The results of our study differ

from their study due to following reasons. (1) The air-sea fluxes (in particular Solar Radiation) we used are based on *in situ* measurements versus their climatological data, (2) the chlorophyll data used to force the model in our study is based on *in situ* measurements versus their climatological counter part, (3) the bio-optical model used in the present study is spectrally resolved versus their non-spectral model.

The difference of the simulation S1w from the simulations S1a (see Fig. B.4) indicates that the mixed layer depth (MLD) lowers by 8 m during the NE monsoon, and during the SW monsoon when the role of chlorophyll is accounted for, compared to a constant clear water situation. During both these periods the impact on the sea surface temperature (SST) is insignificant: less than 0.3 ^{0}C month^{-1}. In contrast, during the spring inter-monsoon, the mixed layer is shallow (MLD $\leq$ 20 m), and the impact of chlorophyll on SST is relatively large: 0.5 ^{0}C month^{-1}. The biological heating impact with respect to the clear-water condition is relatively larger than the impact with respect to constant low background chlorophyll concentration, however, our interest is to asses the impact of seasonal variation of chlorophyll concentration in controlling the upper ocean thermal structure at work.

When the impact of chlorophyll variation on SST is compared to the impact of advective processes[1] (see Fig. B.5), it turns out that the impact of chlorophyll variation is negligible during both the monsoons, whereas these two impacts have similar amplitude during the spring and Autumn inter-monsoons. Similarly the impact of chlorophyll variation on the MLD is negligible (is only 5%) as compared with the impact of advective processes. On the whole, in spite of a 20 fold variation in chlorophyll concentration (0.1 - 2.0 mg m^{-3}, see the Fig. 3.7), its local impact on the 1D physical structure can be neglected.

[1]Note: The heating impact due to advective processes are calculated using S2d, and S1 simulations following the same procedure as done for the impact of chlorophyll in S1a and S1b simulations.

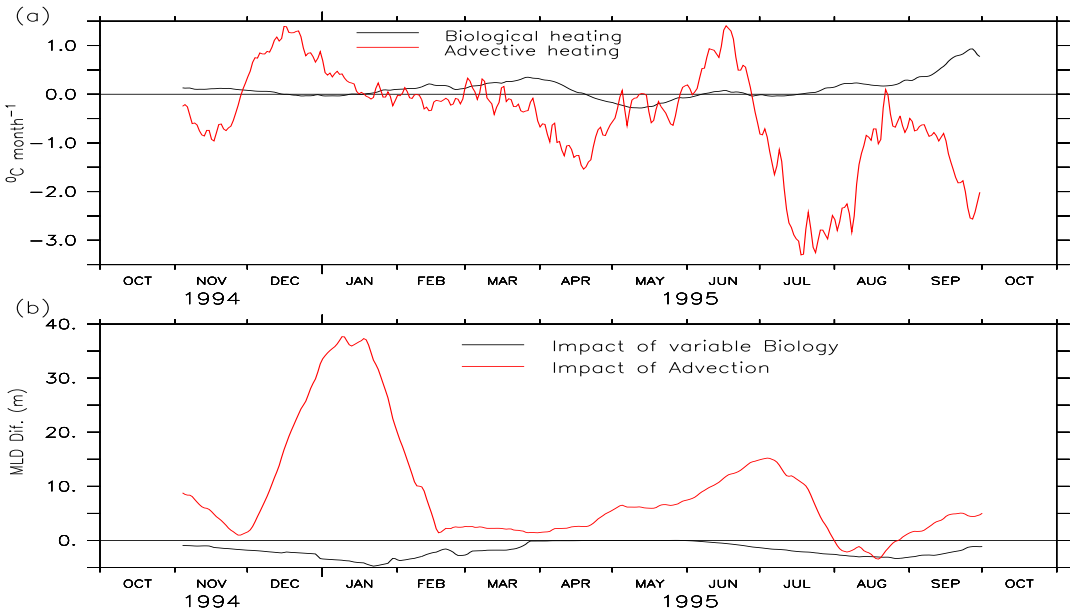

Figure B.5: A comparison between the biological heating effect and advective heating effect contributed to the observed temperature structure at the study location.

B.3 Model sensitivity to the air-sea fluxes

The surface forcing fluxes used in the model were computed from the measurements at the moorring (Weller et al. [2]) at high resolution. It is interesting to know, how sensitive are the model results to the surface forcing fluxes. This issue is now examined by varying arbitrarily the surface forcing fluxes.

B.3.1 ML sensitivity to wind-stress

Two simulations are carried out by forcing the model with modified surface fluxes. The first considers a 10% increase in the wind stress (S1Wa) and the second a 10% decrease in the wind stress (S1Wb). The results of this simulations are compared with the results of the simulation S1 in Fig. B.6. As shown, the deepening of the ML and cooling of the SST enhances with the increase in wind stress. The ML deepening and the SST cooling are different in different periods of the year depending on the strength of the wind stress. Thus, the ML deepening and the SST cooling responding to a 10% increase in the wind stress is not significant (change in SST is less than 0.1 ^{0}C and change in MLD is 1m) during the NE monsoon (period of weak wind) and during the Spring IM (period of moderate wind) excepted for a few occasions of higher deepening of the ML

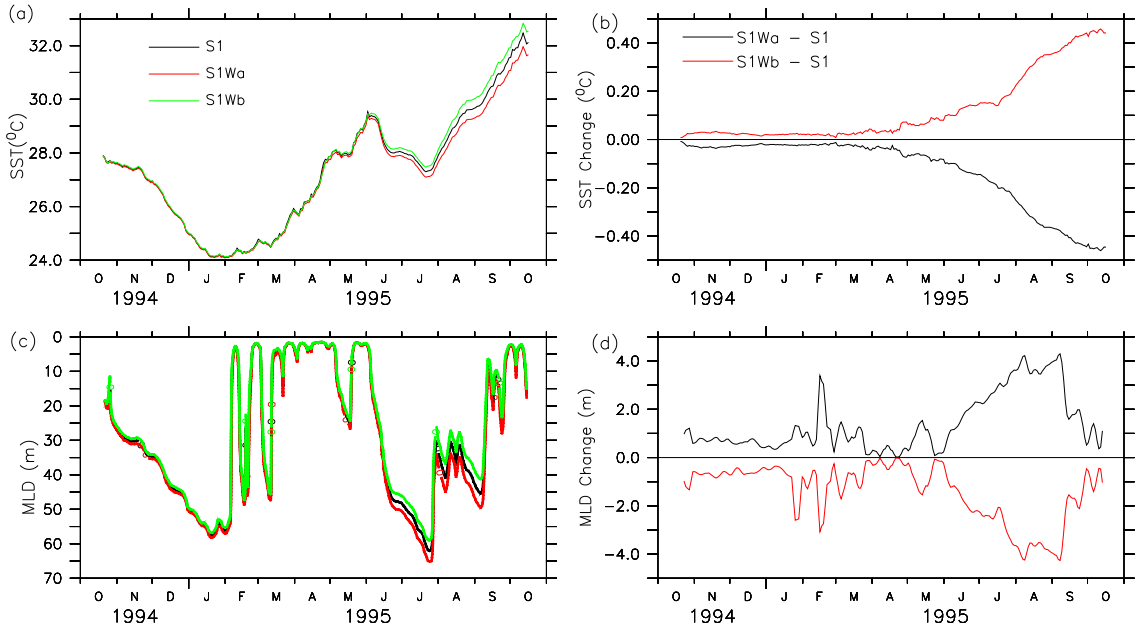

Figure B.6: Results of the sensitivity experiments corresponding to change in the strength of wind stress: S1, the case of exact wind stress; S1Wa, the case of increase in the wind stress by 10%; S1Wb, the case of decrease in wind-stress by 10%.

(3m). The impact of 10% change of wind stress in ML is significant during the SW monsoon (the period of strong wind stress). During this period, the deepening of the ML enhances upto 5m and the cooling of SST enhances upto .5 ^{0}C. The results are exactly symmetric when the experiment is carried out for a 10% decrease in the strength of wind stress. When all these simulations are compared with the observation, the results of the simulation S1 are the best.

In summary, the SST and the MLD predicted by the model for the cases of 10 % increase and decrease in the strength of observed wind field do not differ significantly throughout the year.

B.3.2 ML sensitivity to surface heat fluxes

Solar heat flux

Two simulations of temperature structure are carried out (similar to the S1 experiment) by changing only the solar heat fluxes by 10% keeping the remaining fluxes unchanged. The first simulation (S1Sa) is based on a 10% increase in the solar radiation, and the second simulation (S1Sb) is based on a 10% decrease in solar radiation. The results of the simulations are compared with the results

of the simulation S1 for the case of the exact surface fluxes in the Fig. B.7. The predicted SST and MLD of the simulation S1Sa and S1Sb differ significantly from the S1 prediction. The SST of S1Sa (S1Sb) continuously overestimated (underestimated) than the SST of S1. The MLD of S1Sa (S1Sb) remain shallower (deeper) than the MLD of S1. However, the extent of overestimation (underestimation) in predicted SST and in MLD of S1Sa (S1Sb) are different in different periods of the year depending on the variation in observed solar fluxes. As regarding the increase (decrease) in solar radiation, the extent of the warming (cooling) of SST and the shallowing (deepening) of ML depend on the variability of the solar heat fluxes. During early two months of the NE monsoon (Nov-Dec) the cooling of the SST reduced (enhanced) by 2 ^{0}C and the deepening of ML reduced (enhanced) by 10 m. During January and Spring IM, the enhancement (reduction) in the warming of SST is very significant (4 ^{0}C) but the enhancement (reduction) in the deepening of ML though significant (upto 25 m), are mostly episodic. Unlike the early NE monsoon period, during early two months of the SW monsoon (Jun-July), the cooling in SST was enhanced (reduced) by 2 ^{0}C. During August and subsequent periods of simulation, the warming of SST was enhanced (reduces) by 3 ^{0}C and shallowing (deepening) of ML enhanced by 5 m. When all these simulations are compared with the observation, S1 gives the best results.

In summary, a 10 % change (increase and decrease) in the observed solar radiation can brings significant differences in the predicted surface layer temperature structures (SSTs and MLDs).

Model sensitivity to non-solar surface heat fluxes

The results in the case of 10% increase (decrease) in non-solar heat fluxes are exactly same as the results of the simulation in the case of 10% decrease (increase) in solar radiation.

B.3.3 Causes of general trends of the ML during both the monsoons

During both the monsoons the ML deepens and SST decreases; during the IMs, the ML shallows and SST increases. Weller et al. [3] suggest that the NE monsoon deepening of the ML is driven by convective entrainment and the SW monsoon deepening of the ML is driven by wind mixing. In contrast, earlier studies (McCreary [83], Düing and Leetma [76]) suggested that the SW monsoon ML deepening of the north Arabian Sea is driven by convective entrainment. Therefore the above issues need re-examination. The following experiments are carried out.

1. Very low wind experiment: (wind strength is reduced by 100 times i.e., ~0 m/sec).

2. Very low wind and reduced latent heat flux: (the same wind as in exp. 1 and the latent heat

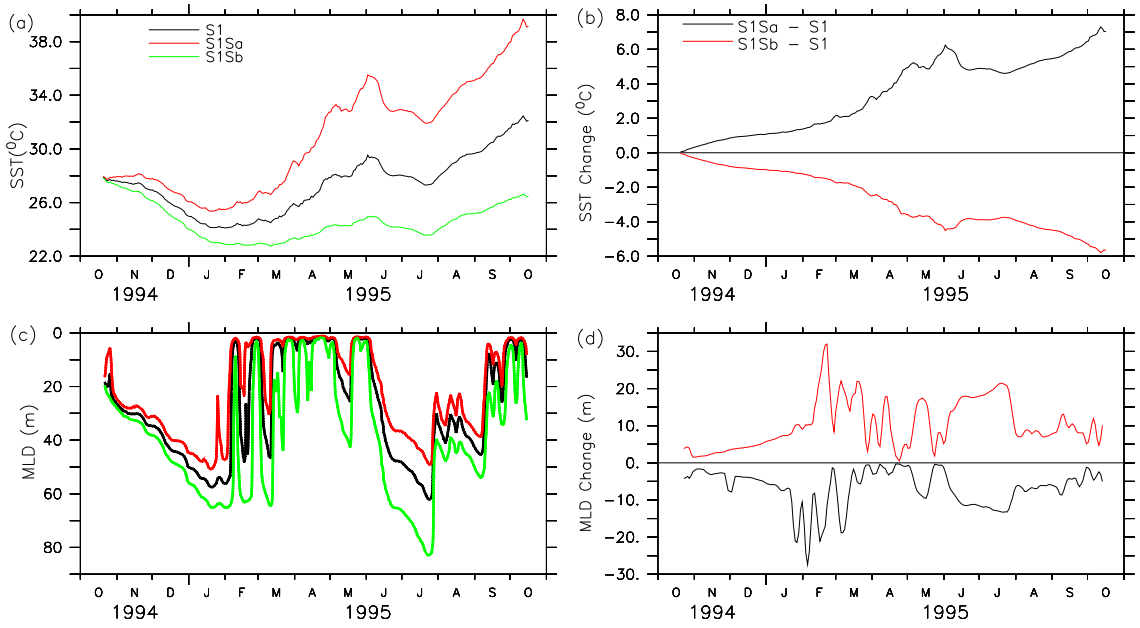

Figure B.7: Results of the sensitivity experiments corresponding to 10% change in the strength of solar radiation: S1, the case of exact solar heating; S1Sa, the case of increase in solar heating; S1Wb, the case of decrease in solar heating.

is reduced by four times)

Low wind experiment

The temperature simulation (W000) of the TKE model is carried out for the light wind condition. The remaining surface fluxes are kept same as in S1. The predicted SST and MLD of W000 are compared with the predicted SST and MLD of S1 in Fig. B.8. As shown, the SST of W000 coincides with the SST of S1 until the arrival of the SW monsoon. During the same period, the MLD of W000 does not differ much from MLD of the simulation S1. When the SW monsoon progresses, W000 started overestimating the SST (over S1) with slower rate for first two months (June-July) and after then the SST of W000 is overestimated rapidly. The evolution of predicted MLD of simulation W000 is underestimated significantly (almost 50 % of S1) during first two months of the SW monsoon. After July, MLD of W000 is reduced to zero during the rest of the year.

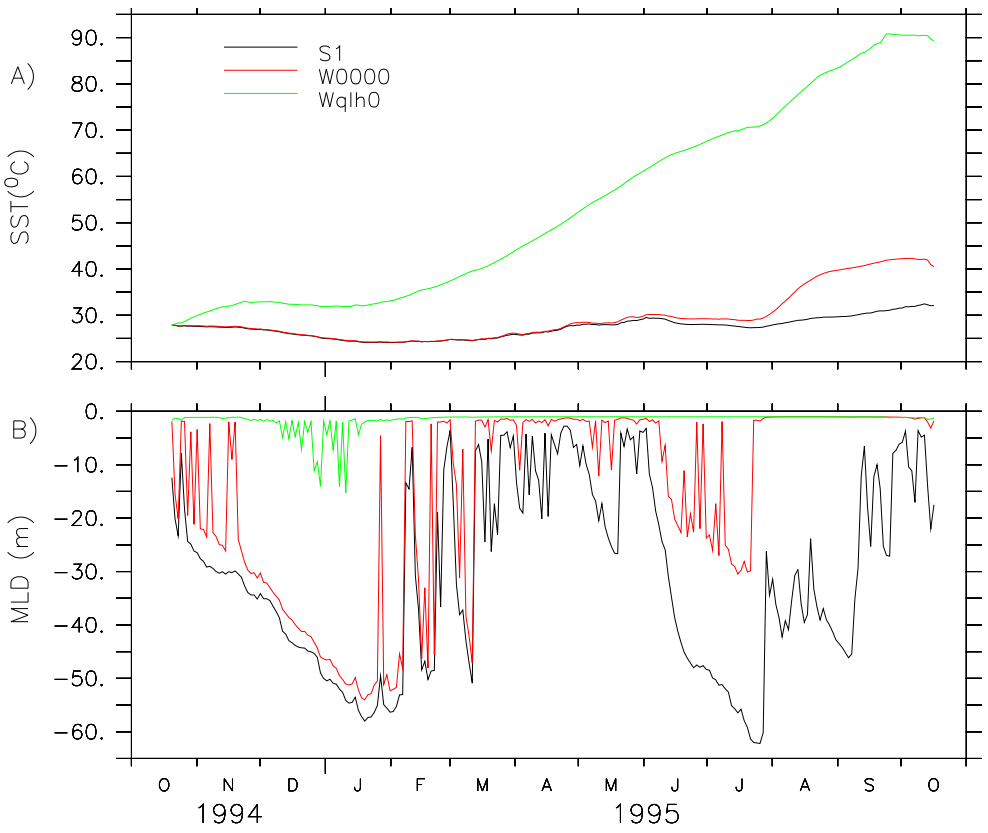

Figure B.8: The results of the simulations carried out to examine the causes of most general trends in the observed MLD and in the observed SST: (A) predicted SST and (B) predicted MLD from the simulations S1 (the case of exact surface wind stress and heat fluxes), W0000 (the case of with negligible wind stress with no change in surface heat fluxes), Wqlh0 (the case of reduced wind stress and reduced net heat loss).

These results show that wind mixing has secondary (minor) role on deepening and cooling of the ML during the NE monsoon, which implies that the surface heat flux must drive the winter cooling and deepening of ML. Further, the simulation shows that the deepening of ML and cooling of SST during early two months of the SW monsoon are not caused by wind stress only, mixing driven by net heat loss at the surface also play role too. During the subsequent period, only wind driven mixing has a significant control over the ML and SST.

Low wind and low heat loss experiment

Now the temperature simulation (Wqlh0) is carried out for the light wind and low heat loss condition. The remaining surface fluxes are kept the same as in S1 (see the Chapter 3.3). The result of this simulation is compared with the simulations S1 and W000 in Fig. B.8. As shown, the predicted SST overestimates the observation throughout the whole year. The ML is reduced to zero throughout the year of the simulation except for the period during December-January, when MLD

is about 10-15 m. This experiment confirmed that deepening of the ML and cooling of the SST during the NE monsoon are mostly due to convective entrainment driven by net buoyancy (heat) loss at the air-sea interface. This also confirmed that the June-July ML deepening and SST cooling are driven by combined effects from wind driven mixing as well as mixing driven by buoyancy (heat) loss at the air-sea interface.

B.4 Conclusion

(1) The numerical experiments corresponding to the salinity and seasonal evolution of biomass (chlorophyll) concentration show that the upper ocean thermal structure in the central Arabian Sea is weakly dependent on these two parameters. (2) Experiments with atmospheric fluxes show that the main trend in the deepening of the ML and cooling of the SST during the NE monsoon are due to a convective entrainment mixing driven by net heat loss at the surface (as a consequence of excess latent heat loss and reduced solar radiation). Contrary to what was proposed by Weller et al. [3] the main trends in deepening of the MLD and the cooling of the SST during the SW monsoon are not only caused by the rapid turbulent mixing driven by wind stress.

Appendix C

Bio-optical models of solar irradiance

A number of bio-optical models of solar irradiance were constructed for various applications to predict under-water light field. In the following, these models are presented in hierchical order (simple to complex).

The vertical attenuation of solar irradiance I(z) is parameterized according to Paulson and Simpson [101] as

$$I(z) = I(0) \times (R \times \exp(-z/\xi_1) + (1 - R) \times \exp(-z/\xi_2)) \tag{C.1}$$

Here, subscripts 1 and 2 refer to the red and, blue-green, parts of the penetrating solar light and z is depth, positive downward. In this equation, R is a dimensionless parameter, and ξ_1 and ξ_2 are attenuation coefficients. Between these two attenuation coefficients, ξ_2 is dependent on phytoplankton (biomass) concentration. In the absence of biomass profile, sensitivity experiments are carried out against various optical water types as proposed by Jerlov's [102] to select constant parameters.

In most part of the oceans biomass dominates the attenuation of penetrating light. About half of the solar insolation incident on the sea surface is absorbed within the top meter. The remaining short-wave radiation of blue-green light decreases exponentially with depth following the Lambert-Beer law. Phytoplankton (biomass) is one of the principal absorbers of visible radiation in the sea. The penetration of light, distribution of under-water light field, absorption and scattering properties of the light in oceanic waters mainly depends on the constituents present in the water column. The light available for photosynthesis at different depths depends on a complete spectral and angular distribution of under water light field and the absorption and scattering properties of pure and oceanic waters. This was extensively dealt with, in photo-synthesis and light in

aquatic ecosystems by Kirk [113]. Sathyendranath and Platt [114] studied the spectral irradiance of light at the surface and in the water. They extensively studied the interaction of light field with chlorophyll its absorption its effect on temperature distribution using spectral and non-spectral, uniform and non-uniform biomass models. In view of above finding, equation (1) can be modified as

$$I(z) = I(0) \times \left(R \times \exp(-z/\xi_1) + (1-R) \times \exp(-\int K\, dz) \right) \tag{C.2}$$

In the simplest case, can $K(1/\xi_2)$be assumed to spectral independent taken as

$K = 0.0611 + 0.0233 \times Chl$ Sathyendranath and Platt [114],

$K = 0.027 + 0.014 \times Chl$ Kirk [113], or

$K = 0.04 + 0.0088 \times Chl + 0.0054 \times Chl^{2/3}$ Parsons et al. [115],

where Chl is chlorophyll concentration (mg m^{-3}). For the spectral-dependent case the attenuation of solar irradince can be written as

$$\begin{gathered} I(z) = I(0) \times \left(R \times \exp(-z/\xi_1) + \textstyle\sum_{r=1}^{r=61} R'_{\lambda_r} \times \exp(-\int K_{\lambda_r} dz) \right) \\ \textstyle\sum_{r=1}^{r=61} R'_{\lambda_r} = 1 - R \\ K_{\lambda_r} = K w_{\lambda_r} + \chi_{\lambda_r} \times Chl^{e_{\lambda_r}} \end{gathered} \tag{C.3}$$

where R'_{λ_r}s are calculated based on the Reference Solar Spectral Irradiance: Air Mass 1.5 (between 400-700 nm for every five nm interval normalized to whole spectral range) (from: http://rredc.nrel. gov/solar/spectra/am1.5/), and Kw_{λ_r}, χ_{λ_r}, and $e_{\lambda_r}$are taken from Table 2 of Morel & Maritorena [111].

The relative performance of these bio-optical model in predicting the under-water light field are presented in Fig. C.1. As shown in figure, three cases of uniform chlorophyll concentration are considered: low (0.1 mg m^{-3}), moderate (0.5 mg m^{-3}), and high (2.0 mg m^{-3}). Predicted I(z) from spectral model (par-spectral) decays much faster than the non spectral model (par - non spectral) in the ocean for all three chlorophyll concentration. For pure oceanic water (no chlorophyll and no other turbid materials) I(z) (parw- spectral) can penetrate much deeper (the photic depth, i.e., 1% of light level lies much below 150 m). Thus choosing the optical model to study the mixed-layer processes is very crucial.

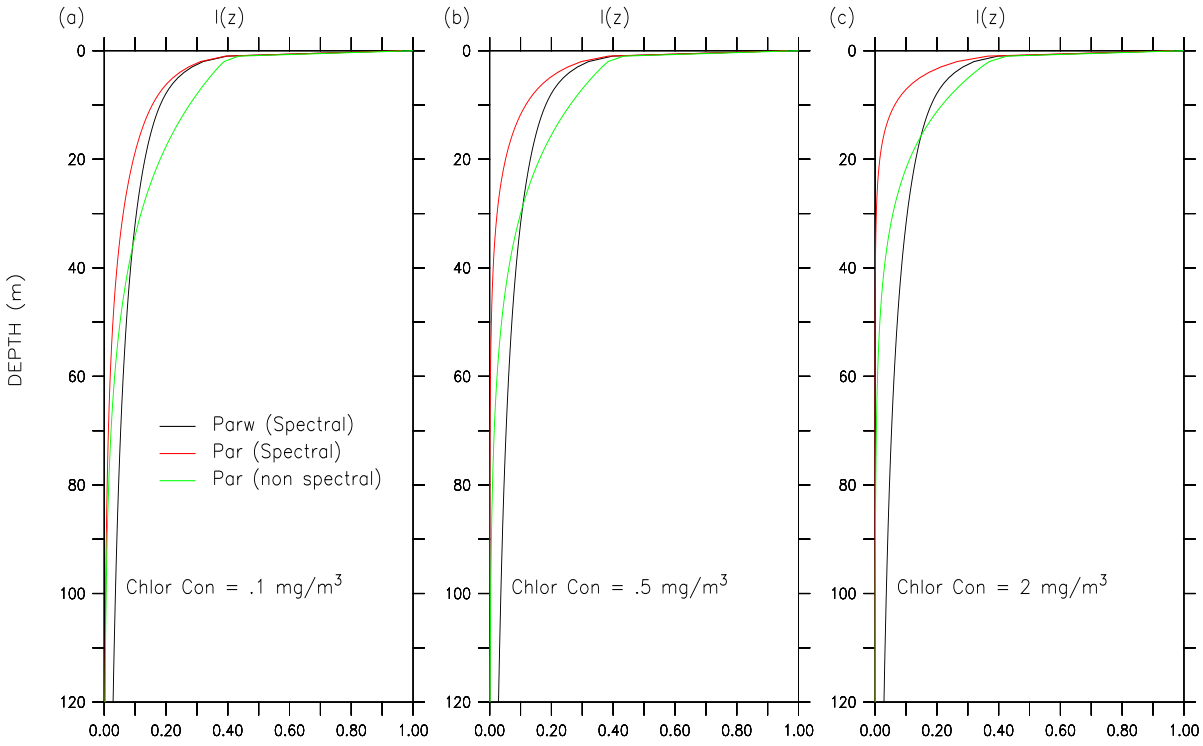

Figure C.1: Under-water solar irradiance predicted from spectral and non spectral bio-optical model for three cases of uniform Chlorophyll concentration: (a) 0.1 mg m^{-3}, (b) 0.5 mg m^{-3}, and (c) 2 mg m^{-3}(see the text for detail).

Appendix D

Additional simulations

D.1 Simulation S2a*: Fischer-based forcing

Simulation of temperature field is carried out by initializing the model on 15 November instead of 20 October (S2a*) similar to S2a. As seen in Fig. D.1, the thermal structure predicted in S2a* is better than in the previous simulation S2a. The predicted SST (Fig. D.1a) parallels the observations throughout the year and the agreement is much better than in S1 during the SW monsoon and during the subsequent period owing to heat removal through the horizontal advection (see Fig. 3.10). The predicted MLD (Fig. D.1b) is not as good as in S2a, but better than in S1. The deepening of ML is significantly underestimated (25 m) during the NE monsoon, and then the prediction almost parallels the observation. The evolution of predicted vertical temperature profile (Fig. D.1c) and the difference between the predicted and observed temperature (Fig. D.1d) show that the temperature of the near-surface layer (upper 40 m) parallels the observation throughout the year, but the temperature in sub-surface (40-160 m) is underestimated. The underestimates are large (7 °C) during the SW monsoon and subsequently. The predicted temperature trend (see Fig. D.1e) mostly matches the observations (Fig. 3.3c). The difference between the predicted and observed temperature trend (Fig. D.1f) is only significant (more than 4 W m^{-3}) in the sub-surface layers during the monsoonal periods.

In summary, the results of above temperature simulations (S2a and S2a*) show that the Fischer et al. [4] estimates of horizontal heat fluxes are not able to improve the model prediction during the early NE monsoon (20 October to mid November-1994). The enormous cooling, driven by horizontal advection of the near-surface layer during this period dominates the model prediction during the rest of the year. Thus, this cooling signal in the horizontal advective heat estimates is suspect. During the rest of the year, the estimates of horizontal heat fluxes may be considered

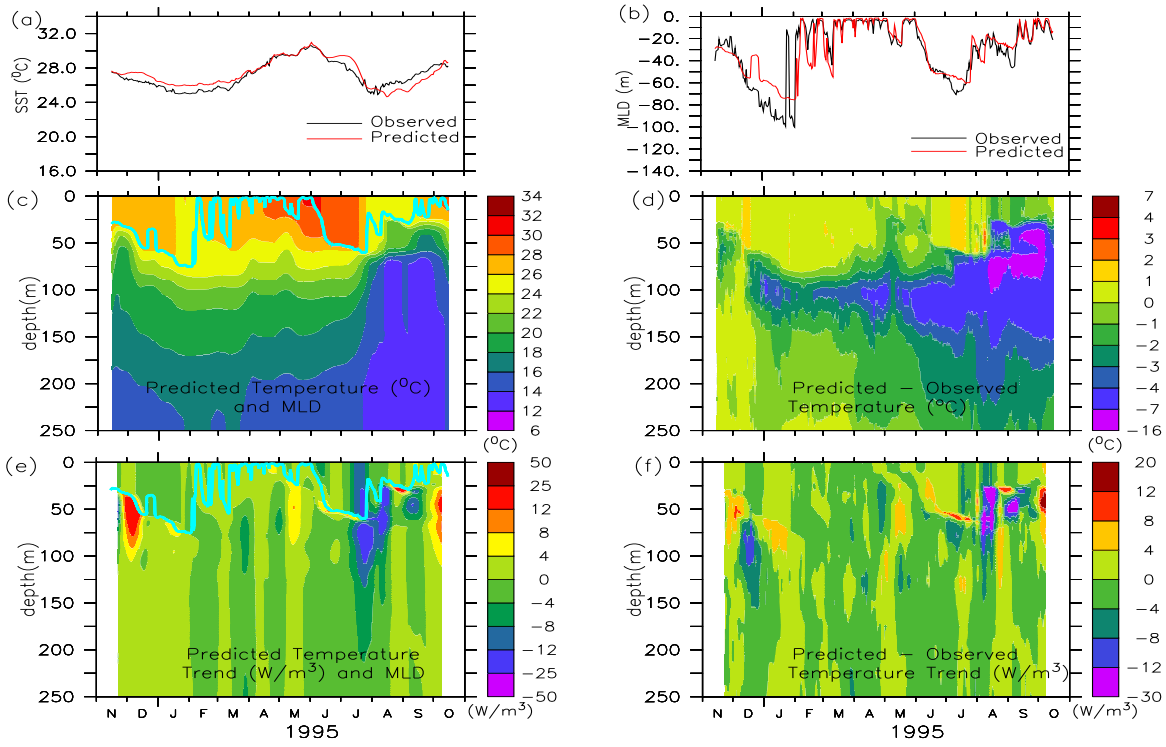

Figure D.1: Results of the numerical simulation S2a*: (a) predicted (red) and observed (black) SST; (b) predicted (red) and observed (black) MLD; (c) vertical structure of temperature (color) and MLD (blue line); (d) predicted minus observed temperature; (e) vertical structure of predicted temperature trend (color) and MLD (blue line); (f) predicted minus observed temperature trend. The data are smoothed as in Fig. 4.1.

as good. Use of the advective field (during mid-November 1994 to mid-October 1995) improved the model prediction significantly in the near-surface layer during the SW monsoon and distorted strongly in the sub-surface due to strong episodic events of the cooling and warming trends associated with it. This implies, the role of vertical advection or the estimates of horizontal advective fluxes might carries much stronger signals than the real signals in the sub-surface layers.

D.2 Simulation S2d: Fischer-based forcing

A simulation (S2d) is carried out similar to the simulation S2c, but the model is initialized on 15 November 1994. The new simulation (S2d) is good and predicted the temperature structure very accurately throughout the year over all depths.

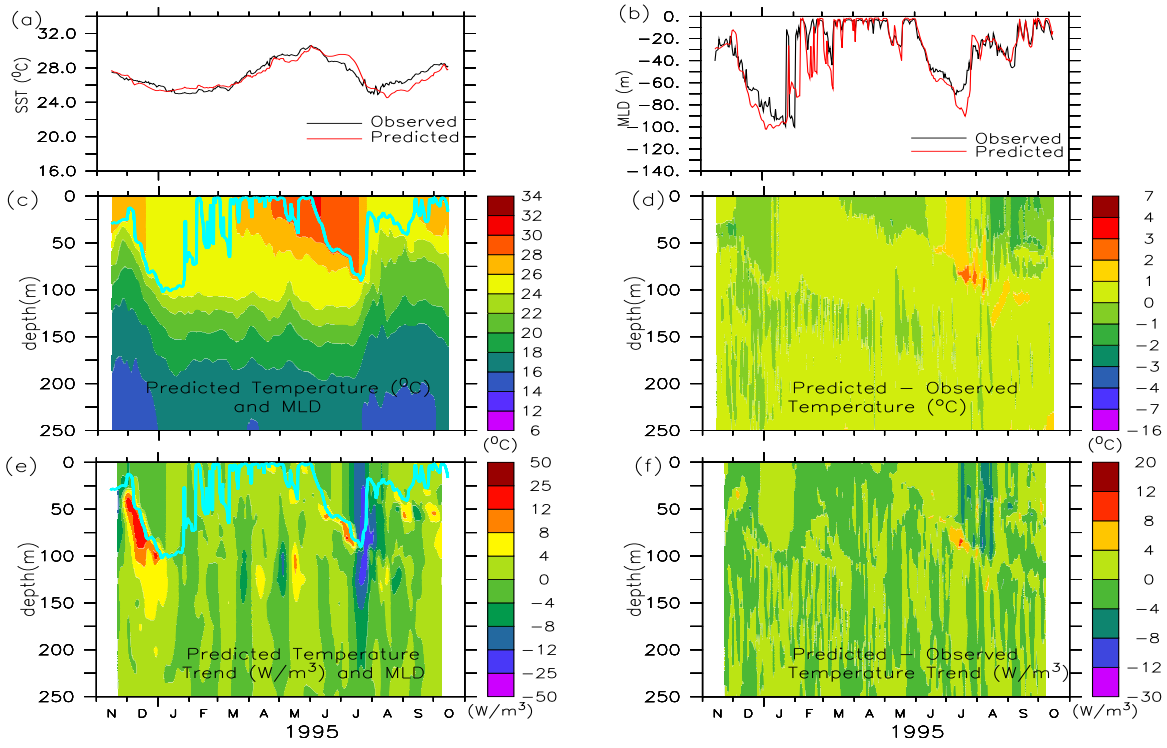

Figure D.2: Results of the numerical simulation S2d: (a) predicted (red) and observed (black) SST; (b) predicted (red) and observed (black) MLD; (c) vertical structure of predicted temperature (color) and MLD (blue line); (d) modeled minus observed temperature; (e) vertical structure of predicted temperature trend (color) and MLD (blue line); (f) predicted minus observed temperature trend. The data are smoothed as in Fig. 4.1.

Appendix E

Estimation of vertical velocity from temperature profile

E.1 Theoretical background

Total vertical velocity $w = w_c + w_A$, where w_C and w_A are the cross and along the iso-line (isopycnal/isotherm) component of the vertical velocity. The cross-isothermal component of vertical velocity is due to two diapycnal processes: (i) heating by penetrating solar radiation and (ii) small scale vertical mixing (Gourious and Reverdin , 1992). At the depth below the mixed-layer and below the photic zone, effect of penetrating solar radiation and small scale mixing process are very small, therefore w_C is negligible (much smaller than 0.1 m d^{-1}, which follows from the scale anlysis by Friedrichs and Hofmann [110] 2001).

The along-isoline component of vertical velocity is due to two effects: (i) local upward movement of isoline $\left(\frac{\partial \eta}{\partial t}\right)$ and (ii) advection along a stationary, sloping isoline $\left(u\frac{\partial \eta}{\partial x} + v\frac{\partial \eta}{\partial y}\right)$:

$$w_A = \frac{\partial \eta}{\partial t} + u\frac{\partial \eta}{\partial x} + v\frac{\partial \eta}{\partial y} \qquad (1)$$

where $\eta = \eta(x, y, t)$ is the elevation of isoline.

Let us assume that the deeper ocean (below the mixed layer) is geostrophic, i.e.

$$\begin{cases} u = -\frac{1}{\rho f}\frac{\partial p}{\partial y} \\ v = \frac{1}{\rho f}\frac{\partial p}{\partial x} \end{cases} \qquad (2)$$

As ocean is hydrostatic , i.e. $\frac{\partial p}{\partial z} = -\rho g \Rightarrow \int_{p_0}^{p} \partial p = -\int_{\eta}^{z} \rho g \partial z \Rightarrow$

$$p = p_0 + \rho g(\eta - z) \qquad (3)$$

Where $p_0 = p_0(x, y)$ is the pressure on the surface of iso-line which is the sum of the pressure at the free surface ($p_a(x, y)$) and pressure due to over laying water mass ($\rho g(H_0 - \eta)$, where $H_0(x, y)$ be the thickness of the fluid layer in the absence of motion (see the Fig. 1)

$$p_0 = p_a + \rho g(H_0 - \eta) \qquad (4)$$

Using eq (4) in eq (3)

$$p = p_a + \rho g(H_0 - z) \qquad (5)$$

Now uses of eq (2 and 3) in eq (1), yields

$$w_A = \frac{\partial \eta}{\partial t} + \frac{1}{\rho f}\left(\frac{\partial(p_a + \rho g H_0)}{\partial x}\frac{\partial \eta}{\partial y} - \frac{\partial(p_a + \rho g H_0)}{\partial y}\frac{\partial \eta}{\partial x}\right) \qquad (6)$$

As $P_a \ll \rho g H_0$ (for an instant at 10 m depth $\rho g H_0$is approximately 10^4time of P_a= 1atmo)

$$w_A = \frac{\partial \eta}{\partial t} + \frac{g}{f}\left(\frac{\partial H_0}{\partial x}\frac{\partial \eta}{\partial y} - \frac{\partial H_0}{\partial y}\frac{\partial \eta}{\partial x}\right) \qquad (7)$$

In the normal mode of oscillation (small oscillation), it can be assumed that $H_0(x, y)$ can varies linearly with $\eta(x, y)$ i.e.

$$H_0(x, y) = \alpha \eta(x, y) \qquad (8)$$

Where α is a constant. Using equation (8) in second expression of right hand side of equation (8), we have

$$\frac{\partial H_0}{\partial x}\frac{\partial \eta}{\partial y} - \frac{\partial H_0}{\partial y}\frac{\partial \eta}{\partial x} = 0 \qquad (9)$$

Therefore equation (7) become

$$w_A = \frac{\partial \eta}{\partial t} \qquad (10)$$

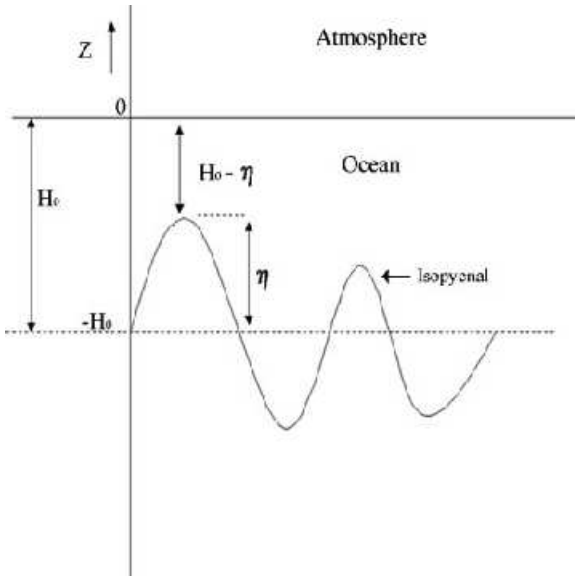

Figure E.1: Schematic of vertical movement of isopycnal

E.2 Estimation of vertical velocity at the moored-array observation

In situ vertical velocity is estimated from the mooring temperature profiles as follows. The profiles are averaged over 5 days. The shift during two consecutive 5-day periods is estimated for two layers, 100–160 m and 180–240 m by using a least-squares fit. This shift is assumed to be due to the vertical velocity field. The vertical velocities are estimated at the centre of each layer and are assumed to be 0 at the surface (rigid-lid approximation). The vertical velocity at other depths in the interval 0–250 m layer is estimated by using linear interpolation and extrapolation using these three values. By averaging the profiles over 5 days, the high-frequency signals (dominant semi-diurnal tide, diurnal tide, and inertial gravity waves) are filtered out. Our estimate of vertical velocity is dependent on the assumption that vertical movement of water controls the vertical changes in temperature profiles. The assumption is consistent with the linear quasi-geostrophic approximation (see Pedlosky [116], pages 67–70). The estimate is expected to be more suitable at sub-surface levels, below the mixed layer and below the photic zone (depth up to which solar short-wave radiation can penetrate), where this assumption is better obeyed. Our method of estimating the vertical velocity is similar to that of Friedrichs and Hofmann [110] (see Appendix-B). The resulting vertical velocities are presented in Fig. E.2. The strength of this vertical velocity is up to 0.003 cm s^{-1} (equivalent to 2.6 m day^{-1}; contrast this with the 18 m day^{-1} estimate of Fischer et al. [4]). As shown, the general trends resemble those in SODA, with downwelling prevailing until the end of the NE monsoon, weak vertical movements from February to June, and active upwelling during the SW monsoon. However, the in situ W exhibits more short-scale variability than in

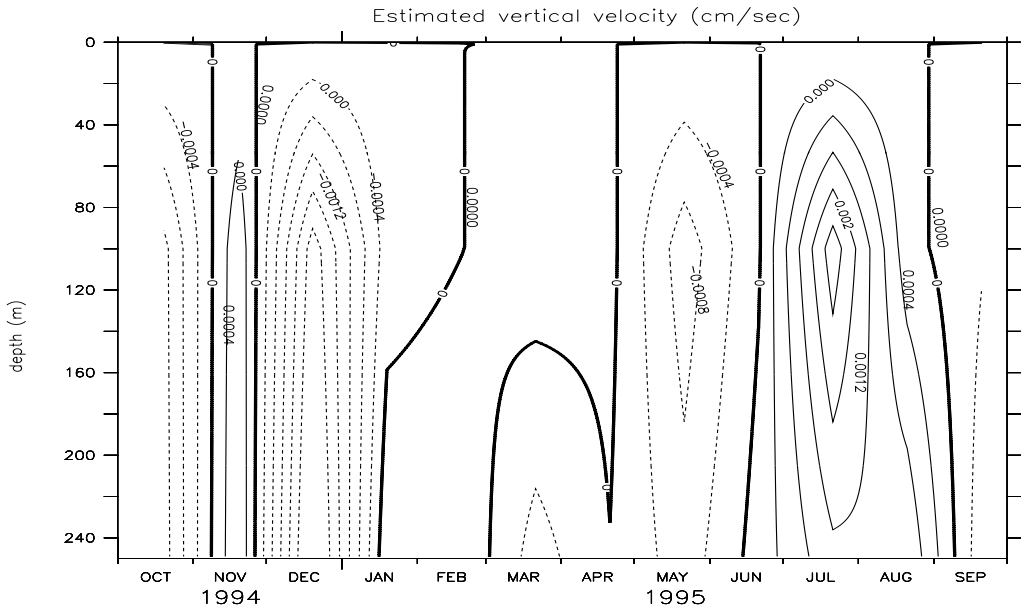

Figure E.2: Contours of vertical velocity (cm/s) based on vertical shift on temperature profile.

SODA. In particular, the downwelling reversed to upwelling from early to late November. Strong downwelling events occur in May and mid-August in sub-surface layers. The July upwelling is much stronger than predicted by SODA. Almost the same estimate of vertical velocity could be obtained by measuring the vertical excursion of different isotherms in the sub-surface layers.

E.3 Examining the vertical velocity (WT) based on T-shift (simulation S3d)

As the vertical velocity from SODA-OGCM is suspected for lacking the small-scale variability, another estimates of vertical velocity (WT) is estimated in the section **??** based on the vertical shift of the temperature profile. The estimates (WT) are used for the vertical advective corrections of the predicted temperature field. The results of the simulation (S3d) are presented in Fig E.3. This simulation (S3d) shows very good agreement between the prediction and the observations. As regards the SST (Fig. E.3a), it is almost unaffected by the change in forcing vertical velocities. In contrast, the vertical structure (Figs. E.3b-c) now exhibits a variability very similar to that in the observations (Fig. 3.3b), in particular for the thermocline layer and for the MLD, and during the periods of intense meso-scale activity (early November to mid-December and August). The remaining departures (Fig. E.3d) are significantly reduced with respect to S3c until mid-July.

In particular, the transient upwelling in November prevents the sub-surface overestimate present in S3c, and the stronger downwelling in December and the transient downwelling in late May prevent most of the S3c sub-surface underestimates. It is after the peak of the SW monsoon that the improvements are the least apparent, with mis-estimates still present in surface (+3 °C) and in sub-surface layers (-2 °C). It is also worth noting that, once the problems which occur in S3c during the NE monsoon have been settled, the thermal structure is well reproduced throughout the inter-monsoon. The most of the warming and cooling trends in the sub-surface are reproduced well (Fig. E.3e-f). Over the year, the mean temperature in the mixed layer differs from the observed mean by -0.28 °C and the temperature profiles are simulated with an accuracy of 2.14$\pm$1.58 % (mean $\pm$ standard deviation) in terms of absolute relative error while the mean temperature difference is -0.18 °C and the accuracy is (2.72$\pm$2.15 %) for the 0 - 250 m layer. The trend in the predicted temperature was integrated over the ML and over the 0 - 250 m layer for S3d. They are compared to the observed trend in Fig. E.4 (in units of heat flux). As shown, this simulation reproduces most of the observed features for both layers. It has, however, to be noted that the model failed to reproduce a few short-term events. These events (a few days long) occurred mainly in January and during the SW monsoon, concerned the whole layer (Fig. E.4 lower panel), and had a marked signature in the ML (Fig. E.4 upper panel).

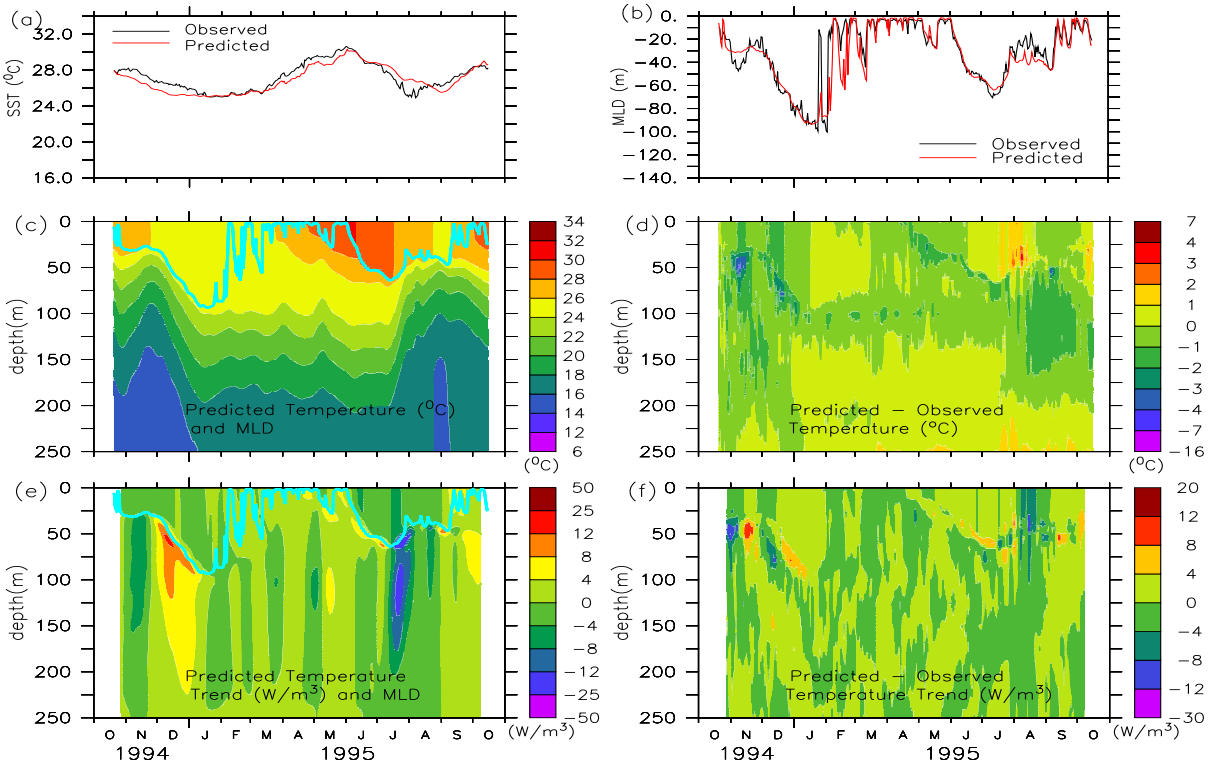

Figure E.3: Results of the numerical simulation S3d: (a) predicted (red) and observed (black) SST; (b) predicted (red) and observed (black) MLD; (c) vertical structure of predicted temperature (color) and MLD (blue line); (d) modeled minus observed temperature; (e) vertical structure of predicted temperature trend (color) and MLD (blue line); (f) predicted minus observed temperature trend. The data are smoothed as in Fig. 4.1.

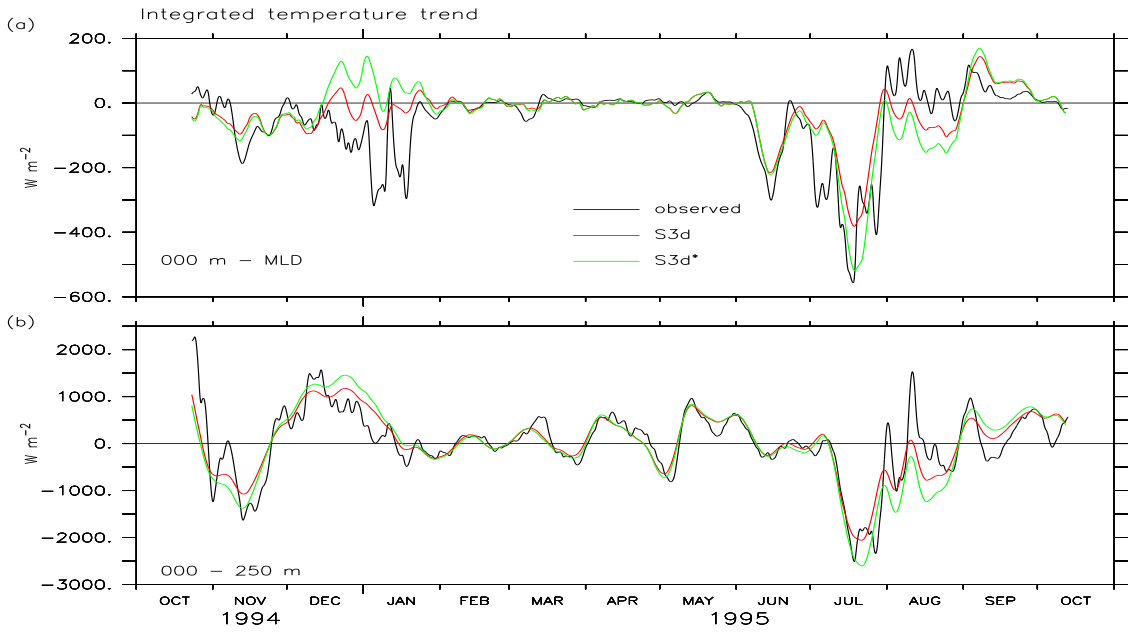

Figure E.4: Evolutions of the observed (black) and the modeled (red) temperature trend integrated over the ML (upper panel) and over the 0-250 m layer (lower panel) for S3 experiment.

Appendix F

Additional figures

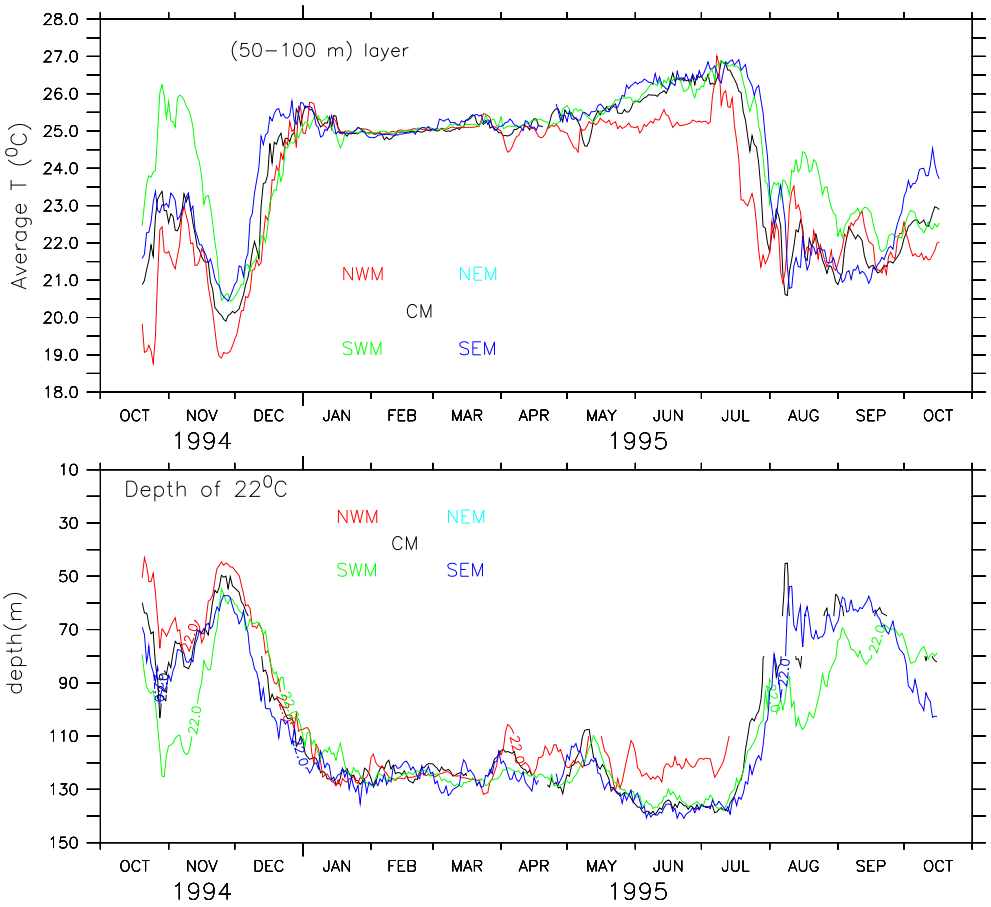

Figure F.1: Averaged temperature evolution between 50 and 100 m (upper panel) and depth of 22°C iso-therm from the four moorings (lower panel). Dark color: central mooring (CM); red color: north west mooring (SWM); green color: south west mooring (SWM); and blue color: south east mooring (SEM); cyan color: north east mooring (NEM) which was missed. During November of the NE monsoon and August of the SW monsoon (August) the SWM shows large differences from other mooring.

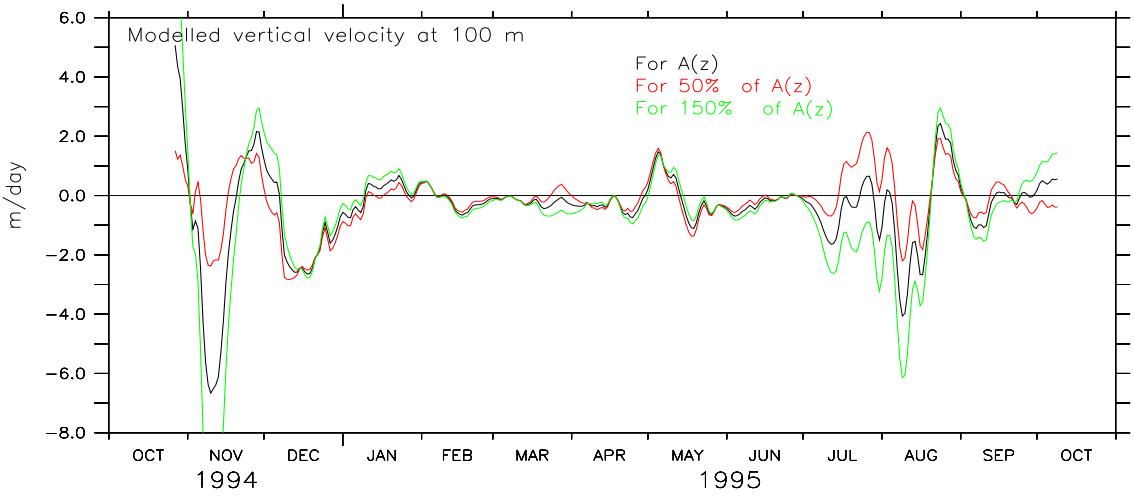

(a)

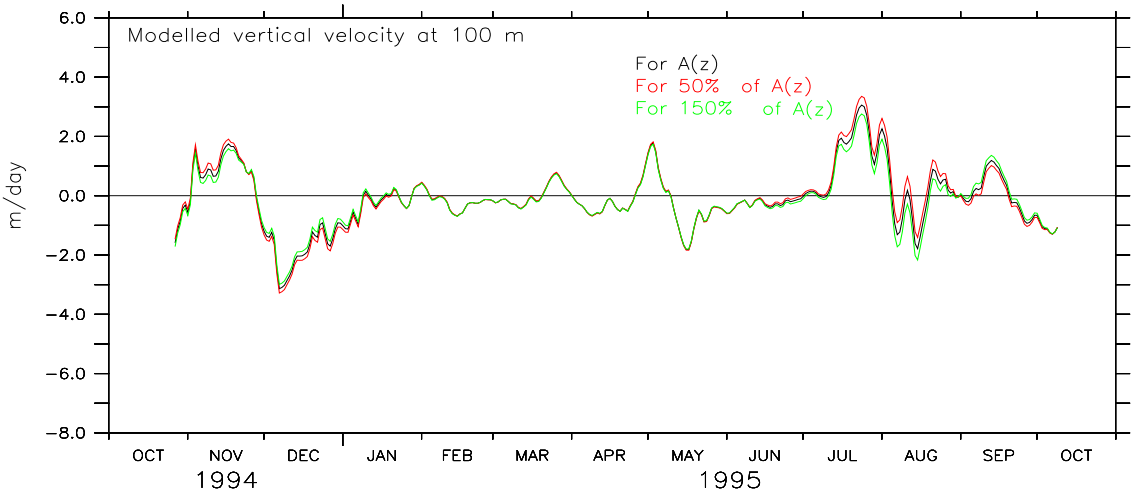

(b)

Figure F.2: (a) Sensitivity of predicted vertical velocity to the Fischer-based horizontal advective heat fluxes. (b) same as (a) but with respect to Reynolds-based horizontal advective heat fluxes.

Bibliography

[1] Findlater, J., 1969. A major low-level air current near the Indian Ocean during the northern summer. *Quaterly Journal of the Royal Meteorological Society*, 95: 362–380.

[2] Weller, R. A., M. F. Baumgartner, S. A. Josey, A. S. Fischer, and J. C. Kindley, 1998: Atmospheric forcing in the Arabian Sea during 1994-1995: observation and comparisons with climatology, and models. *Deep-Sea Research II* 45: 1961–1999.

[3] Weller, R. A., A. S. Fischer, D. L. Rudnick, C. C. Eriksen, T. D. Dickey, J. Marra, C. Fox, R. Leben, 2002. Moored Observations of upper-ocean response to the monsoon in the Arabian Sea during 1994-1995. *Deep Sea Research II* 49: 2195–2230.

[4] Fischer, Albert S., R. A. Weller, D. L. Rudnick, C. C. Eriksen, C. M. Lee, K. H. Brink, C. A. Fox, and R. R. Leben, 2002. Mesoscale eddies, coastal upwelling, and the upper-ocean heat budget in the Arabian Sea. *Deep Sea Research II* 49: 2231–2264.

[5] Peixoto, J. P. and A. H. Oort, 1992: Physics of Climate. *Americal Institute of Physics*, 500 pp.

[6] Houghton, J.T., L.G. Meira Filho, B.A. Callender, N. Hariris, A. Kattenberg, and K. Maskell, 1995. The science of climate change, (eds) *Cambridge University Press*, Cambridge, UK.

[7] Mitchell, J. M., 1976: An overview of climatic variability and its causal mechanisms. *Quaternary Research*, 6: 1–13.

[8] Oceanography Course Team, 2001. Ocean Circulation, Second edition, *The Open University*.

[9] Bjerknes, J. A, 1966. Possible response of the atmospheric Hardley circulation to equatorial anomalies of ocean temperature. *Tellus*, 18: 820–829.

[10] Bjerknes, J., 1969. Atmospheric tele-connections from the equatorial Pacific. *Monsoon Weather Review*, 97: 163–172.

[11] Gray, W. M., 1968. Global view of the origin of tropical disturbances and storms. *Monthly Weather Review*, 96: 669-700.

[12] McBride, J., 1995. Tropical cyclone formation (chapter 3), Global Perspectives on Tropical Cyclones. *Ed. R. L. Elsberry*, World Meteorological Organisation Report WMO/TD-693: 63–105.

[13] Briegel, L. M. and Frank W. M., 1997. Large-scale influences on tropical cyclogenesis in the western North Pacific, *Monsoon weather Review*, 125: 1397–1413.

[14] Lindzen. R.S., and S. Nigam, 1987. On the role of sea surface temperature gradients in forcing low-levl wind and convergence in the Tropics. *Journal of Atmospheric Science*, 44: 2418–2436.

[15] Gray, W. M., 1984. Atlantic seasonal hurricanes frequency. Part 1: El Niño and 30 mb quasi-biennial oscillation influences. *Monthly Weather Review*, 112: 1649–1668.

[16] Goldenberg, S. B., and Shapiro, L.J., 1996. Physical mechanisms for the association of El Niño and west African rainfall with Atlantic major hurricane activity. *Journal of Climate*, 9: 1169–1187.

[17] Lander, M. A., 1994. An exploratory analysis of the relationship between tropical storm formation in the western Pacific and ENSO. *Monsoon Weather Review*, 122: 639–651.

[18] Chan J.C.L., 2000. Tropical cyclone activity over the western North Pacific associated with El Niño and La Niña events. *Journal of Climate*, 13: 2960–2972.

[19] Chu, P.S. and Wang, J., 1997. Tropical cyclones occurrences in the vicinity of Hawaii: are the difference between El Niño and non-El Niño years significant? *Journal of Climate*, 10: 2683–2689.

[20] Hastings, P. A., 1990: Southern Oscillation influences on tropical cyclones activity in the Australian/south-west Pacific region. *International Journal of Climatology*, 10: 291–298.

[21] Evans, J. L., and Allan, R. J., 1992. El Niño/Southern Oscillation modification to the structure of the monsoon and tropical cyclone activity in the Australasian region. *International Journal of Climatology*, 12: 611–623.

[22] Basher, R. E. and Zheng, X., 1995: Tropical cyclones in the southwest Pacific: spatial patterns and relationships to Southern Oscillation and sea surface temperature. *Journal of Climate*, 8: 1249–1260.

[23] Broadbridge, L.W. and Hanstrum, B.N., 1998. The relationship between tropical cyclones near Western Australia and the Southern Oscillation index. *Australian Meteorological Magazine*, 47: 183–189.

[24] Gray, W.M. LAD, 1994. Multiple linear regrassion forecasts of Atlantic tropical storm activity for 1995. *Experimental Long-lead Forecast Bulletin*, 3: 12–13.

[25] Elsner, J.B., G.S. Lehmiller, and T.B. Kimberlain, 1996. Early August forecasts of Atlantic tropical storm activity for the balance of the 1996 season, using Poisson models. *Experimental Long-lead Forecast Bulletin*, 5: 26–38.

[26] Chan, J.C.L, J.E. Shi, and C.M. Lam, 1998. Seasonal forecasting of tropical cyclone activity over the western North Pacific and the South China Sea. *Weather and Forecast*, 13: 997–1004.

[27] NOAA, 2002. www. pmel.noaa.gov.

[28] Vialard, J., and P. Delecluse, 1998. An OGCM study for the TOGA decade. Part I: Role of salinity in the Physics of the Western Pacific Fresh Pool. *Journal of Physical Oceanography*, 28: 1071–1088.

[29] Levitus S. and T.P. Boyer. 1994. World Ocean Atlas 1994 Volume 4: Temperature. NOAA Atlas NESDIS 4. 117 pp.

[30] Sprintall, J., and M. Tomczak, 1992. Evidence of the barrier layer in the surface layer of tropics. *Journal of Geophysical Research,* 97: 7305–7316.

[31] Delcroix, T., G. Eldin, M.-H. Radenac, J. Toole, and E. Firing, 1992. Variation of the western equatorial Pacific, 1974-1988, Journal of Geophysical research, 97 (Suppl.): 3249–3262.

[32] Sprintall, J., and M. J. McPhaden, 1994. Surface layer variations observed in multi year time series measurements from the western equatorial Pacific. *Journal of Geophysical Research*, 99: 963–979.

[33] Vialard, J., and P. Delecluse, 1998. An OGCM study for the TOGA decade. Part II: Barrier-Layer Formation and Variability, *Journal of Physical Oceanography*, 28: 1089–1106.

[34] Shenoi, S. S. C., D. Shankar, and S. R. Shetye, 2002. Differences in heat budgets of the near-surface Arabian Sea and Bay of Bengal: Implications for the summer monsoon. *Journal of Geophysical Research* 107 C6, 10.1029/2000JC000679.

[35] Durand, F., S. R. Shetye, J. Vialard, D. Shankar, S.S.C. Shenoi, C. Ethe, and G. Madec, 2004. Impact of temperature inversions on SST evolution in the southeastern Arabian Sea during the pre summer-monsoon season, *Geophysical Research Letter*, 31, L01305, doi:10.1029/2003 GL018906.

[36] Sathyendranath, S., A. D. Gouveia, S. R. Shetye, and T. Platt, 1991. Biological controls of surface temperature in the Arabian Sea. Nature, 349: 54–56.

[37] Gadgil, S., P. V. Joseph and M. V. Joshi, 1984. Ocean-atmosphere coupling over monsoon regions. *Nature*, 31: 141–143.

[38] Webster, P.J., T. Palmer, M. Yanai, V. Magan, J. Shukla, R. A. Tomas, M. Yanai, and A. Uasunari, 1998: Monsoons: Processes, predictability and the prospects for prediction. *Journal of Geophysical Research*, 103 C7: 14451–14510.

[39] Science Plan of the Indian Climate Research Programme, 1996. *Department of Science and Technology, Government of India, New Delhi*, pp186.

[40] Varadachari, V.V.R., 1990. Oceans and Climate, *Monograph*, Anonymus.

[41] Choudhary, M. H. K and S. Karmarkar, 1982. Diagnostic study on some aspects of the energetics and structural features of the troposhere over the Arabian Sea with advancement of SW monsoon. *In: Results of Summer Monex Field Phase Research (Part B), FGGE Operations Report Vol. 9, ICSU/WMO*: 212–221.

[42] Hastenrath, S., 1985. Climate and circulation of the tropics, *D. Reidel Publishing company, Derdretcht, Holland,* 455 pp.

[43] Hastenrath, S. and Lamb, P. J., 1980. Climatic Atlas of the Indian Ocean Part 2. The Oceanic heat budget. *University of Wisconson Press*, 110pp.

[44] Saha, K.R., 1970. Zonal anomaly of sea surface temperature in the equatorial Indian Ocean and its possible effect upon monsoon circulation. *Tellus*, 22: 403–409.

[45] Saha, K.R., 1974. Some aspects of the Arabian Sea monsoon. Tellus, 26: 464–476.

[46] Rao, L.V.G., V. Ramesh Babu, A.A. Fernandes and V.V.R. Varadachari, 1976. Studies on thennal structure of the northwestern Indian Ocean in reflation to the southwest monsoon over the Indian Peninsula. *In: Proceedings of the symposium on tropical monsoons*. Indian Institute of Tropical Meteorology, Pune, pp. 219.

[47] Rao, A.V.A.K., R.K. Datta, G.S. Mandai and Indu Bala, 1980. Certain aspects of SST and moisture distribution over the Arabian Sea during pre-onset phase of Monsoon 1979. *In: Results of Summer Monex Field Phase Research (part B), FGGE Operations Report Vol. 9 ICSU/WMO*, 167–172.

[48] Nuzhdin, P.V., 1982. On laws covering fluctuations of the Arabian Sea active layer thermodynamics properties and air-sea energy exchange characteristics during the southwest monsoon. *In: GARP International Conference on the scientific results of the monsoon experiment, Bali, ICSU/WMO, Geneva*, 724–727.

[49] Jambunathan, R. and K. Ramamurty, 1975. Sea and air temperature distribution over the Arabian Sea during southwest monsoon, 1973. *Journal of Meteorology and Geophysics*, 26: 465–478.

[50] Anjaneyulu, T.S.S., 1980. A study of the air and surface temperature over the Indian Ocean. *Mausam*, 31: 551–560.

[51] Joseph, P.V., 1981. Seasonal scale persistance of equatorward intrusion of upper tropospheric westerlies over south Asia and monsoon performance dunng 1964 to 1979. *In: GARP International Conference on the Scientific Results of the Monsoon Experiment*. Bali, Indonesia, October 1981. ICSU/WMO, 171–174.

[52] Joseph, P. V., 1981. Ocean-atmosphere interaction on a seasonal scale over north Indian Ocean and Indian monsoon rainfall and cyclone tracks -a preliminary study. *Mausam*, 32: 237–246.

[53] Joseph, P. V. and P. V. Pillai, 1986. Air-sea interaction on a seasonal scale over north Indian Ocean -Part II: Monthly mea" atmopheric and oceamc parameters during 1972 and 1973. *Mausam*, 37: 158–168.

[54] Joseph, P. V., 1976. Monsoon rainfall and cyclone tracks in relation to 500 mb altitudes. 1955–1974. *In: Proceedings of the symposium on tropica1 monsoons*. Indian Institute of Tropical Meteorology, Pune, pp. 494–504.

[55] Joseph, P. V. and P. V. Pillal, 1984: Air-sea interaction on a seasonal scale over the north Indian Ocean -IJI Part I: Interannual variations of sea surface temperature and Indian summer monsoon rainfall. *Mausum*, 35:323–330.

[56] Golovastov, V.A., V.V. Pokudov and V.B. Kholmanov., 1982. Peculiarities of the water thermodynamics in the tropical Indian Ocean. *In: International Conference on the Scientific results of Monsoon Experiment*. Bali, Indonesia, October 1981. ICSU/WMO, 720–723.

[57] Shukla, J. and B.M. Mishra, 1977. Relationships between sea surface temperature and wind speed over the central Arabian Sea and monsoon rainfall over India. *Monthly Weather Review*, 105, 998–1002.

[58] Weare, B.C., 1979. A statistical study of the relationship between ocean surface temperatures and the Indian monsoon. *Journal of Atmospheric Science*, 36: 2279–2291.

[59] Ramesh Kumar, M.R., S. Sathyendranath, N.K. Viswambharan and L. V.G. Rao, 1986. Sea surface temperature variability over North Indian Ocean, a study of two contrasting monsoon seasons. *Proc. Ind. Acad. Sci. (Earth and Planetary Science)*, 95: 435–446.

[60] Ramesh Kumar, M.R., Sadhuram, Y. and L.V.G. Rao, 1986. Premonsoon sea surface temperature anomaly off the "western Indian Ocean. A probable predictor for monsoon rainfall; Presented at the Seminar on Long-range "forecasting of monsoon rainfall", *India Meteorological Society*, New Delhi, April 16–18.

[61] Cadet, D.L. and B.C. Diehl, 1984. Interannual variability of surface field is over the Indian Ocean during recent decades. *Monthly Weather Review*, 12: 1921–1935.

[62] Webster, P. J., 1994. The role of hydrological processes in ocean-atmosphere interaction. *Review of Geophysics*, 32: 427–476.

[63] Washington, W.M., R.M. Chervin and G. V. Rao, 1977. Effects of a variety of Indian Ocean surface temperature patterns on the summer monsoon circulation: Experiments with NCAR general circulation model. *Pure and Applied Geophysics*, 115: 1335–1356.

[64] Druyan, L.M., 1982. Studies of the Indian Summer Monsoon with a coarse-mesh general circulation model, Part I. Journal of Climatology, 1, 127–139

[65] Washington, W.M., 1981. A review of general circulation model experiments on the Indian monsoon. In: Monsoon Dynamics. Edited by J. lighthill and R.P. Pearce, *Cambridge University Press*, London, p. 111–130.

[66] Shukla, J., 1987. Interannual variability of monsoons. In: Monsoons editted by J.S. Fein and P.L. Stephens, *John Wiley and Sons*, New York, pp. 399–463.

[67] Shukla, K. R., and M.J. Fennesssy, 1994. Simulation and predictability of monsoons. Proc. Int. Conf. on Monsoon Variability and Prediction, Tech. Rep. WCRP-84, Geneva, Swizerland, World Climate Research Programme, 567–575.

[68] Shukla, J., 1975. Effect of Arabian Sea surface temperature anomaly on Indian summer monsoon. A numerical experiment with the GFDL model. *Journal of Atmospheric Science*, 32: 503–511.

[69] Kershaw, R., 1988: Effect of sea surface anomaly on a prediction of the onset of the southwest monsoon over India. *Quarterly Journal of Royal Meteorological Society*, 114: 325–345.

[70] Yang, S., and K. M. Lau, 1998. Influence of sea surface temperature and gound wetness on the Asian summer monsoon. *Journal of Climate*, 11: 3230–3246.

[71] Hatenrath, S. and Lamb, P.J., 1980. On the heat budget of hydrosphere and atmosphere in the Indian Ocean. Journal of Physical Oceangraphy, 10: 694–708.

[72] Golovastov, V.A., 1980. Peculiarities of ocean thermodynamics in the tropical Indian Ocean during the southwest monsoon 1979. *In: Results of Summer Monex Field Phase Research (Part B), FGGE Operations Report* Vol. 3, ICSU/WMO, 186–192.

[73] Golovastov, V.A., V.V. Pokudov and V.B. Kholmanov., 1982. Peculiarities of the water thermodynamics in the tropical Indian Ocean. *In: International Conference on the Scientific results of Monsoon Experiment*. Bali, Indonesia, October 1981. ICSU/WMO, 720–723.

[74] Wyrtki, K., Benonett, E.B., and Rochford, D.J., 1971. Oceanographic Atlas of the International Indian ocean Expedition, N.S.F., Washington, D.C., pp. 1–531.

[75] Colborn, J., 1976. The thermal structure of Indian Ocean, *The University Press of Hawaii*, Honolulu. 177 pp.

[76] Düing, W., A. Leetmaa, 1980. Arabian Sea cooling. a preliminary heat budget. *Journal of Physical Oceanography,* 10: 307–312.

[77] Sastry, J.S. and V. Ramesh Babu, 1984. Summercooling of the Arabian Sea - A review. *Proceedings of the Indian Academy of Sciences (Earth and Planetary Sciences)*, 94: 117–128.

[78] Murty, V.S.N., D.P. Rao and J.S. Sastry, 1983. The lowering of sea surface temperature in the east central Arabian Sea. *Mahasagar -Bulletin of the National Institute of Oceanography*, *Goa*, 16, 67–71.

[79] Shetye, S. R., 1986. A model study of the seasonal cycle of the Arabian Sea surface temperature. *Journal of Marine Research,* 44: 521–542.

[80] Kraus, E. B., and J. S. Turner, 1967. A one-dimensional model of the seasonal thermocline: II. The general theory and its consequences. *Tellus*, 19, 98–106.

[81] Denman., K. L., 1973. A time-dependent model of the upper ocean, *Journal of Physical Oceanography* 3, 173–184.

[82] Rao, R. R., 1986. Cooling and deepening of the mixed-layer in the central Arabian Sea during MONSOON-77: observation and simulation. *Deep-Sea Research A* 33: 1413-1424.

[83] McCreary, J. P., Jr., P. K. Kundu, and R. L. Molinari, 1993. A numerical investigation of dynamics, thermodynamics and mixedlayer processes in the Indian Ocean. *Progress in Oceanography*, Vol. 31, Pergamon, 181–244.

[84] Wacogne, S., Pacanowski, R., 1996. Seasonal heat transport in a primitive equations model of the tropical Indian Ocean. *Journal of Physical Oceanography* 26: 2666–2699.

[85] Loschning, J., and P. J. Webster, 2000. A coupled ocean-atmosphere system of SST modulation for the Indian Ocean, *Journal of Climate* 13: 3342–3360.

[86] Sigurdson, D.E., T. Dickey, D. Manov, 1995. Arabian Sea Mooring Data report: Deploiment # 1 October 15, 1994–April 20, 1995. Ocean Physics Laboratory, Santa barbara.

[87] Sigurdson, D.E., T. Dickey, D. Manov, 1996. Arabian Sea Mooring Data report: Deploiment # 2 April 22–October 20, 1995. *Ocean Physics Laboratory*, Santa barbara.

[88] Dickey, T.D., J. Marra, D. E. Sigurdson, R. A. Weller, S.S. Kinkade, S.E. Zedler, J.D. Wiggeri, C. Langdon, 1998. Seasonal variability of bio-optical and physical properties in the Arabian Sea: October 1994 - October 1995. *Deep Sea Research II*, 45: 2001–2025.

[89] Price, James F., Robert A. Weller, and Robert Pinkel, 1986. Diurnal cycling: Observations and models of the upper ocean response to diurnal heating, cooling, and wind mixing. *Journal of Geophysical Research*, 91(C7): 8411–8427.

[90] Gaspar, P., 1988. Modeling the seasonal cycle of the upper ocean. *Journal of Physical Oceanogaphy*, 18: 161–180.

[91] Mellor, G. L., and T. Yamada, 1974. A hierarchy of turbulence closure models for planetary boundary layers, *Journal of Atmospheric Science*, 31: 1791–1806.

[92] Bougeault, P., and P. Lacarrere, 1989. Parameterization of orography iduced turbulence in a meso-beta scale model, *Monthly Weather Review*, 117: 1872–1890.

[93] Gaspar, P., Y. Gregoris, and J. M. Lefevre, 1990. A simple Eddy Kinetic Energy Model for simulation of the Oceanic Vertical Mixing: Tests at station Papa and Long-Term Upper Ocean Study Site. *Journal of Geophysical Research* 95 C9: 16179–16193.

[94] Mellor, G. L., and T. Yamada, 1982. Development of a turbulence closure model for geophysical fluid problems, *Review of Geophysics*, 20: 851–875.

[95] Galperin, B., A. Rosati, L.H. Kantha, and G.L. Mellor. 1989. Modeling rotating stratified turbulent flows with application to oceanic mixed layers. *Journal of Physical Oceanography*, 19: 901–916.

[96] Levy, M., L. Memery and J-M. Andre, 1998. Simulation of primary production and export fluxes in the Northwestern Mediterranean Sea. *Journal of Marine Research* 56: 197–238.

[97] Pondaven P., D. Ruiz-Pino, C., Fravalo, P. Treguer, and C. Jeandel, 2000: Inter-annual variability of Si and N bio-geochemical cycles at the southern Ocean JGOFS station Kerfix, 1990–1995. *Deep-Sea research*, part I 47: 223-257.

[98] Blank, B., and P. Delecluse, 1993. Variability of the tropical Atlantic Ocean simulated by general circulation model with two different mixed layer physics. *Journal of Physical Oceanography* 23, 1363–1388.

[99] Gregg, M.C., H. Peters, J. C. Wesson, N. S. Oakey, and T. J. Shay, 1985. Intensive measurements of turbulence and shear in the equatorial undercurrent, *Nature*, 318, 140–144.

[100] Bougeault, P., and J. C. Andre, 1986. On the stability of the third-order turbulence closure for the modeling of the stratosumulus-topped boundary layer, *Journal of Atmospheric Science*, 43, 1574–1581.

[101] Paulson, C. A., J. J. Simpson, 1977. Irradiance measurements in the upper ocean, Journal of Physical Oceangraphy 7: 952–956.

[102] Jerlov, N. G., 1976. Marine Optics, *Elseveir Oceanography Series*, Vol. 14, 231 pp.

[103] Reynolds, R. W., and T. M. Smith, 1994. Improved global Sea Surface Temperature analysis using optimum interpolation. Journal of Climate 7: 929–948.

[104] Saji, N. H., B. N. Goswami, P. N. Vinayachandran, and T. Yamagata, 1999. A dipole mode in tropical Indian Ocean. *Nature* 401, 360–361.

[105] Sreejith, O. P. and S. S. C. Shenoi, 2002. An evaluation of satellite and in situ based sea surface temperature datasets in the North Indtian Ocean region. *International Journal of Remote Sensing*, Vol. 23, no. 24: 5165–5175.

[106] Carton, James. A., Gennady Chepurin, Xianhe Cao, and Benjamin Giese, 2000. A simple Ocean Data Assimilation Analysis of the Global Upper Ocean 1950-95, Part I: Methodology. *Journal of Physical Oceangraphy* 30: 294–309.

[107] Carton, James A., Gennady Chepurin, Xianhe Cao, and Benjamin Giese, 2000. A simple Ocean Data Assimilation Analysis of the Global Upper Ocean 1950–95, Part II: Results. *Journal of Physical Oceangraphy* 30: 311–326.

[108] ECMWF, European Centre for Medium-Range Weather Forecasts— *http://www.ecmwf.int*

[109] Helber, R. W. and R. H. Weisberg, 2001. Equatorial upwelling in the western Pacific warm pool. Journal of Geophysical Research, 106, C5: 8989 (2000JC000401).

[110] Friedrichs, Marjorie A. M., and Eileen E. Hofmann, 2001. Physical control of biological processes in the central equatorial Pacific Ocean. *Deep-Sea Research* I 48, 1023–1069.

[111] Morel, A., and S. Maritorena, 2001. Bio-optical properties of oceanic waters: A reappraisal. *Journal of Geophysical Research*, 106: 7163–7180.

[112] Babu, K.N., Rashmi Sharma, Neeraj Agarwal, Vijay K. Agrawal, and R. A. Weller, 2004. Study of the mixed layer depth variations within the north Indian Ocean using a 1-D model. *Journal of Jeophysical Research*, Vol. 109, C08016, doi:10.1029/2003JC002024.

[113] Kirk, J. T. O, 1994. Light and Photosynthesis in Aquatic Ecosystems. *Cambridge university press*, 509 p.

[114] Sathyendranath, S. and T. Platt, 1988. The spectral irradiance field at the surface and in the interior of the ocean: A model for applications in Oceanography and remote sensing. Journal of Geophysical Research 93 C8: 9270–9280.

[115] Parsons, T. R., M. takahashi, and B. Hargrave, 1984. Biological Oceanographic Processes, *Pergamon*, New York.

[116] Pedolosky, J., 1979. Geophysical Fluid Dynamics. *Springer*. 624pp.

[117] Fischer, A. S., 1997: Arabian Sea mixed layer deepening during the monsoon: Observation and dynamics. M.S. Thesis. *Masschusetts Institute of Thechnology and Woods Hole Oceanographic Institution*, Woods Hole, Massachusetts, 130 pp.

[118] Bruce, J.G, D. R. Johnson, and J. C. Kindle, 1994: Evidence for eddy formation in the eastern Arabian Sea during the northeast monsoon, Journal of Geophysical Research, 99: 7651–7664.

[119] Keen, T. R., J. C. Kindle, and D. K. Young, 1997. The interaction of southwest monsoon upwelling , advection and primary production in the northwest Arabian Sea, *Journal of Marine System*, 13: 61–82.

[120] Miller, J. R., 1976. The salinity effect in a mixedlayer ocean model, *Journal of Physical Oceanography*, Vol. 6, No. 1: 29-35.

[121] Millero, F.S., and A. Poisson, 1981. An international one-atmosphere equation of state of sea-water. *Deep Sea Research*, 28A, 625–629.

[122] Hastenrath, S., 1982: On meridional heat transports in the World ocean. *Journal of Oceanography*, 12: 922–927.

[123] Barnett, T.P., 1984: Long-term trends in surface temperature over the oceans. *Monthly Weather Review*, 112. 303–312.

[124] Gopinathan, C.K. and J.S. Sastry, 1986. Is the summer monsoon rainfall over India related to the Bay of Bengal SST? Presented at the Seminar on Long-range forecasting of monsoon rainfall, *India Meteorological Society*, New Delhi, April 16–18.

[125] Gopinathan, C.K. and D.P. Rao, 1985. Surface temperature of the Indian Ocean before summer monsoon. *Mahasagar -Bulletin of the National Institute of Oceanography*, Goa, 18: 281–292.

[126] Rochford, Peter A., John C. Kindle, Patrik C. Gallacher, and Robert A. Weller, 2000. Sensitivity of the Arabian Sea mixed layer to 1994-1995 operational wind products. *Journal of Geophysical Research*, Vol. 105, No. C6: 14141–14162.

[127] Pedolosky, J., 1979. *Geophysical Fluid Dynamics*. Springer. 624pp.

[128] Prashad, T. G., 2004. A comparison of mixed-layer dynamics between the Arabian Sea and the Bay of Bengal: One-dimensional model results. *Journal of Geophysical Research*, Vol. 109, C03035, doi:10.1029/2003JC002000.

[129] Ekman, V.W., 1905. On the influence of the earth's rotation on ocean currents. *Ark. Mat. Astron. Fys*. 2, No. 11.

[130] Andreson, S. P., R. A. Weller, and R. B. Weller, 1996. Surface buoyancy forcing and the mixed layer of the western Pacific warm pool: Observations and one-dimensional model results. *Journal of Climate*, 9: 3056–3085.

[131] Kitaygorodskiy, S. A., 1961. On the possibility of theoretical calculation of vertical temperature profile in upper layer of the sea. *Izv. Akad. Nauk SSSR, Ser. Geofiz*., No. 1–6: 313–318.

[132] Adamec, D., R. L. Elsberry, R.W. Garwood, and R. L. haney, 1981. An embedded mixed-layer-ocean circulation model. *Dynamics of Atmosphere and Oceans*, 6: 69–77.

[133] Niller, P.P., and E. B. Kraus, One-dimensional models of the upper ocean, 1977. *Modelling and prediction of the upper layers of the ocean*, edited by E. B. Kraus, pp. 143–172, Pergamon, New York.

[134] Peters, H., M.C. Gregg, and J. M. Toole, 1988. On the parameterization of equatorial turbulence, Journal of Geaphysical research, 93: 1199–1218.

[135] Arakawa, A., 1972. Design of the UCLA general circulation model. Numerical simulation of weather and climate. Technical Report 7, Dept. of Meteorology, University of califernia, Los Angeles, CA, 116 pp.